UNIVERSITY OF CALIFORNIA,
IRVINE

Instrumentation Development for MAS NMR Spectroscopy of Oriented Liquid Samples

DISSERTATION

submitted in partial satisfaction of the requirements
for the degree of

DOCTOR OF PHILOSOPHY

in Physics

by

Kelsey A. Collier

Dissertation Committee:
Professor Rachel W. Martin, Chair
Professor Zuzanna Siwy
Professor Kieron Burke

2016

TABLE OF CONTENTS

LIST OF FIGURES

LIST OF TABLES

ACKNOWLEDGMENTS

I would like to thank Professor Rachel Martin, for teaching me about NMR probes.

Dr. Catalina Espinosa, for teaching me the ins and outs of trying to build a probe from scratch.

Lee Moritz, for teaching me how to machine, and for his cheerful and patient answers to my many questions.

Dr. Suvrajit Sengupta, for teaching me how to use the instrument I was building to take data, and for calling me out on my bad habits in the machine shop before I lost an eye!

John Kelly, for his steady hands and his patience.

CURRICULUM VITAE

Kelsey A. Collier

EDUCATION

Bachelor of Science in Physics **2010**
University of California, Santa Cruz *Santa Cruz, California*

Master of Science in Physics **2016**
University of California, Irvine *Irvine, California*

RESEARCH EXPERIENCE

Graduate Research Assistant **2010–2016**
University of California, Irvine *Irvine, California*

Undergraduate Researcher **2009–2010**
University of California, Santa Cruz *Santa Cruz, California*

TEACHING EXPERIENCE

Teaching Assistant **2010–2014**
University of California, Irvine *Irvine, California*

REFEREED CONFERENCE PUBLICATIONS

Design and Construction of a Four-Channel $^{1}H/^{13}C/^{2}H/^{15}N$ SAS ss-NMR Probe **March 2013**
Experimental Nuclear Magnetic Resonance Conference

Design and Construction of a Four-Channel $^{1}H/^{13}C/^{2}H/^{15}N$ SAS ss-NMR Probe **July 2014**
Rocky Mountain Conference on Analytical Chemistry

ABSTRACT OF THE DISSERTATION

Instrumentation Development for MAS NMR Spectroscopy of Oriented Liquid Samples

By

Kelsey A. Collier

Doctor of Philosophy in Physics

University of California, Irvine, 2016

Professor Rachel W. Martin, Chair

This thesis describes a quadruple-resonance $^{1}H/^{13}C/^{2}H/^{15}N$ magic-angle spinning nuclear magnetic resonance probe for the study of structure and dynamics of biological macromolecules. The probe utilizes tuning-tube components as discrete circuit elements. A coaxial design allows specialization, with the high-frequency ^{1}H circuit on a low-voltage modified Alderman-Grant coil and the $^{13}C/^{2}H/^{15}N$ circuit on a solenoid coil for more efficient detection. The mechanical and circuit design of the probe is presented with a description of the benchtop characterization and some initial experimental results.

Chapter 1

Introduction

1.1 Motivation

There exists a bewilderingly wide variety of proteins serving a variety of different functions. The specificity of their function is determined by their precise three-dimensional structure. The structure of a protein is determined by the bonds formed between the sidechains of its component amino acid residues. This structure is described at up to four levels[3]. The primary structure is the sequence of amino acid residues in the polypeptide chain(s) that form the protein. The secondary structure describes the shapes that different portions of the polypeptide form, commonly α-helices and β-sheets, when the protein folds. The tertiary structure is the overall globular structure of the molecule driven by hydrophobic interactions and stabilized by hydrogen and disulfide bonds.

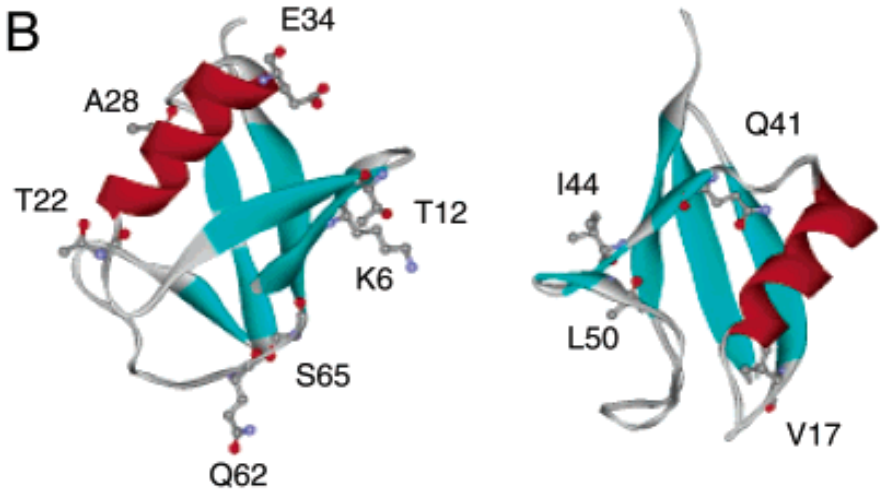

Figure 1.1: Structure of the small protein ubiquitin solved by NMR[1]. The α-helices are shown in red and the β-sheets in teal, with arrows showing the direction of the polypeptide.

The quaternary structure can be used to describe the assembly of multiple proteins into a single structure, again driven by hydrophobic interactions[4].

It is the precise folding of the polypeptide sequence into these complicated structures that allows proteins to catalyze reactions, mediate passage through cell membranes, determine selectivity of immune response, regulate cell growth and differentiation, and serve specific structural functions. Understanding protein structure provides key insights into how these processes work as well as aiding drug design.

The study of protein folding is one of the key areas of structural biology–as is, therefore, the study of protein misfolding[5]. What happens what a protein, due to mutation or damage, has its structure changed? In many cases, the answer is disease. Cystic fibrosis, sickle cell anemia, and some types of cancer result from misfolded proteins[6]; the role of mutation in protein misfoding accounts for the familial nature of these disorders. Other diseases, including cataract, Alzheimer's and Parkinson's diseases, and type II diabetes, result specifically from the aggregation of misfolded proteins[7]. The importance of protein structuure can be seen in the cellular machinery devoted exclusively to consuming misfolded proteins. The prevalence

of these diseases in old age[8] results from the breakdown of this machinery.

The question is, then, which methods are best for these structural studies. For small molecules, solution-state nuclear magnetic resonance (NMR) is commonly used to study structure and interactions. Larger molecules are crystallized and studied with X-ray diffraction.

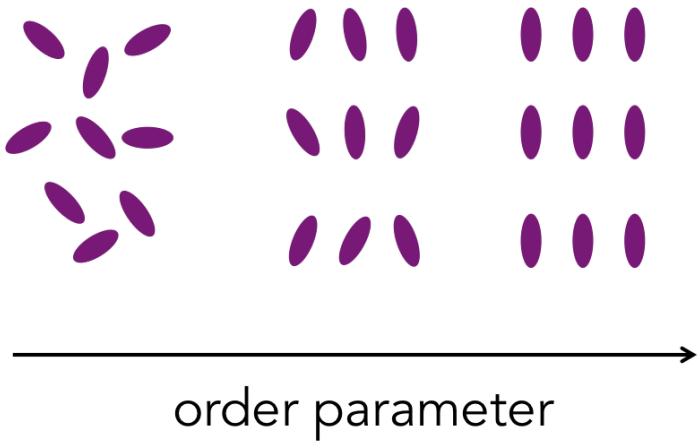

Figure 1.2: Basic schematic of the order parameter continuum.

However, there exist molecules for which neither technique is suited, those which are too large or too oriented for solutions NMR but cannot be crystallized for diffraction measurements. For samples such as membrane proteins, which are embedded in a lipid bilayer in their biologically relevant conformation, there can be concern as to whether crystallization changes their structure [9].

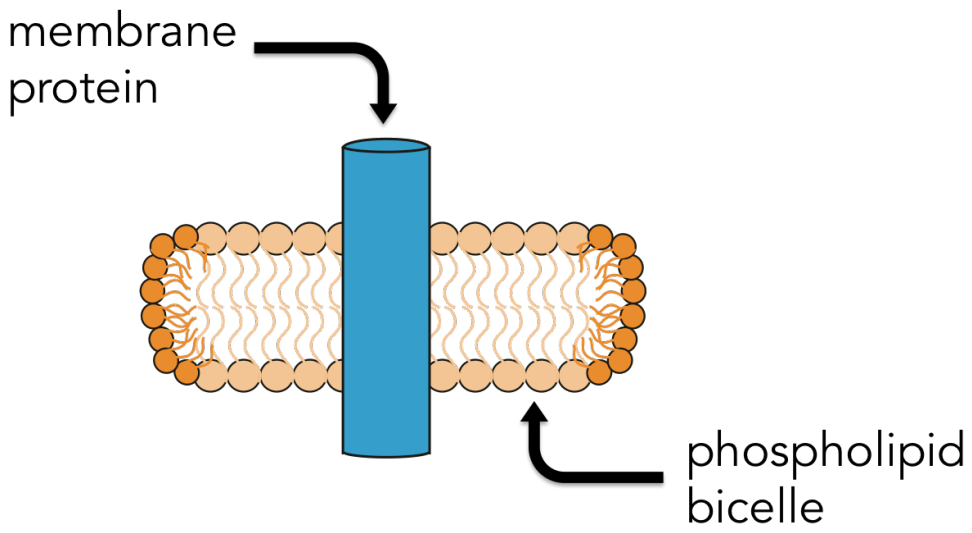

Figure 1.3: Schematic of a membrane protein inserted in a phospholipid bilayer membrane mimetic.

Ideally the structures of these molecules are studied while they are embedded in a membrane mimetic [10]; this system is, of course, too large for the techniques of solution-state NMR to work.

The structures of misfolded proteins are also of interest, especially in those cases in which misfolding causes aggregation. Protein aggregation has been implicated in many diseases, including Alzheimer's disease, type II diabetes, and cataract [5]. Understanding the structural changes that lead to this aggregation is important for the treatment and eventual prevention of these diseases.

Both membrane mimetics and protein aggregates are the kind of large, oriented semisolid samples that the techniques of solid-state NMR are well suited to [11, 12, 13].

1.2 NMR Theory

So what, exactly, is NMR? Nuclear spins with a non-zero quantum number precess in a magnetic field. The Larmor frequency, the frequency of this precession, scales according to:

$$\omega = -\gamma B_0 \tag{1.1}$$

such that it depends on both the strength of the magnetic field and the gyromagnetic ratio of the nucleus. This frequency is a result of the Zeeman splitting resulting from the possible alignment of the z-component of the nuclear spin moments with or against the external field. A set of nuclear spins placed in an intense magnetic field will, due to an induced (small) alignment of the spins, have a precessing magnetic moment. This precessing magnetic field can induce a current in a coil wound around the sample [14, 15].

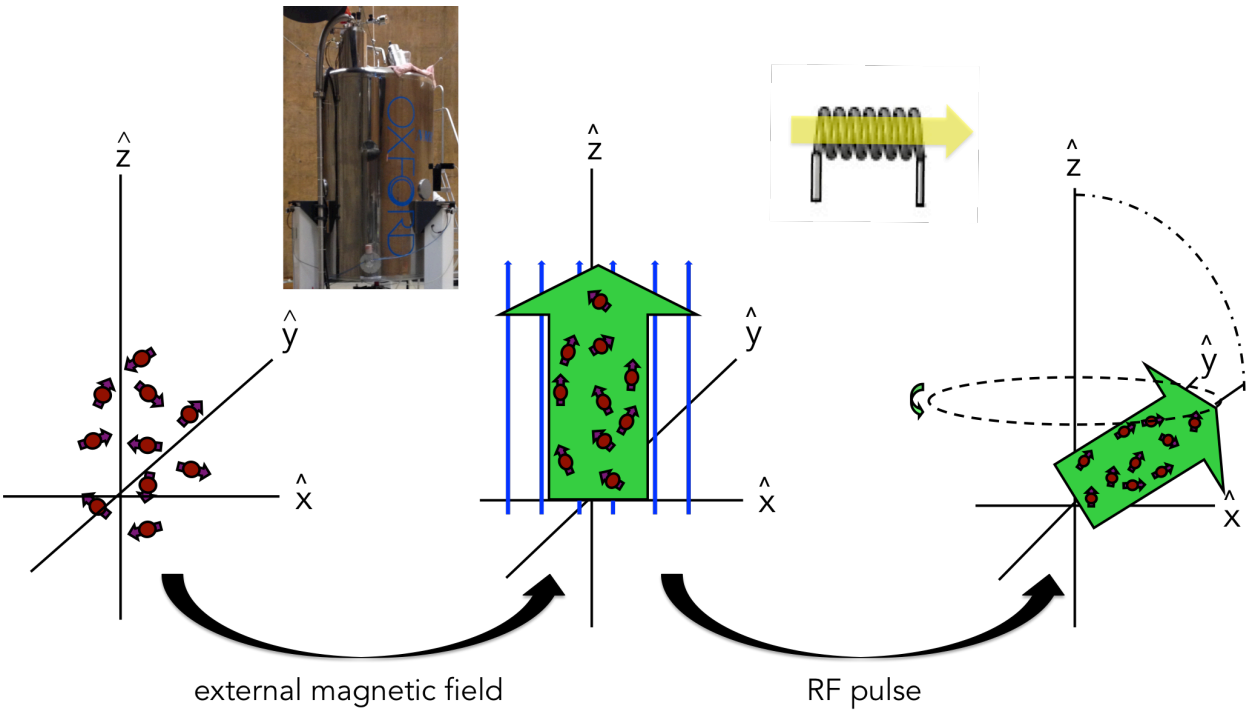

Figure 1.4: The basic mechanism of NMR.

How does this technique allow molecular structures to be determined? Differences in local electronic environment, the distribution of electrons in chemical bonds, result in different nuclei within a molecule experiencing different local magnetic fields. This means that the spins of nuclei in different positions in a molecule precess at slightly different frequencies–the "chemical shift".

$$H = -\hbar\gamma B_0 I_Z[1 - \delta_{iso} - \frac{1}{2}\delta_{CSA}P_2(cos\theta)] \tag{1.2}$$

The Larmor precession frequency is determined by the strength of the external magnetic field and the gyromagnetic ratio of the nucleus, since it results from the Zeeman splitting of

the spin energy levels. This frequency should be constant for all nuclei of the same species–so how could it be used to study structure? Small shifts in this frequency are seen based on the local chemical environment of the spins. The varying electronic shielding causes nuclei of the same type in different bond locations in a molecule to experience slightly different local magnetic fields. This, then, causes a "chemical shift" in the observed precession frequencies. The chemical shift δ has both an isotropic and an anisotropic part, with the anisotropic term dependent on the angle of the sample relative to the external field.

The measured precession frequencies are Fourier transformed and indexed against a reference value, so that data are visualized as a spectrum of intensity as a function of shift in frequency.

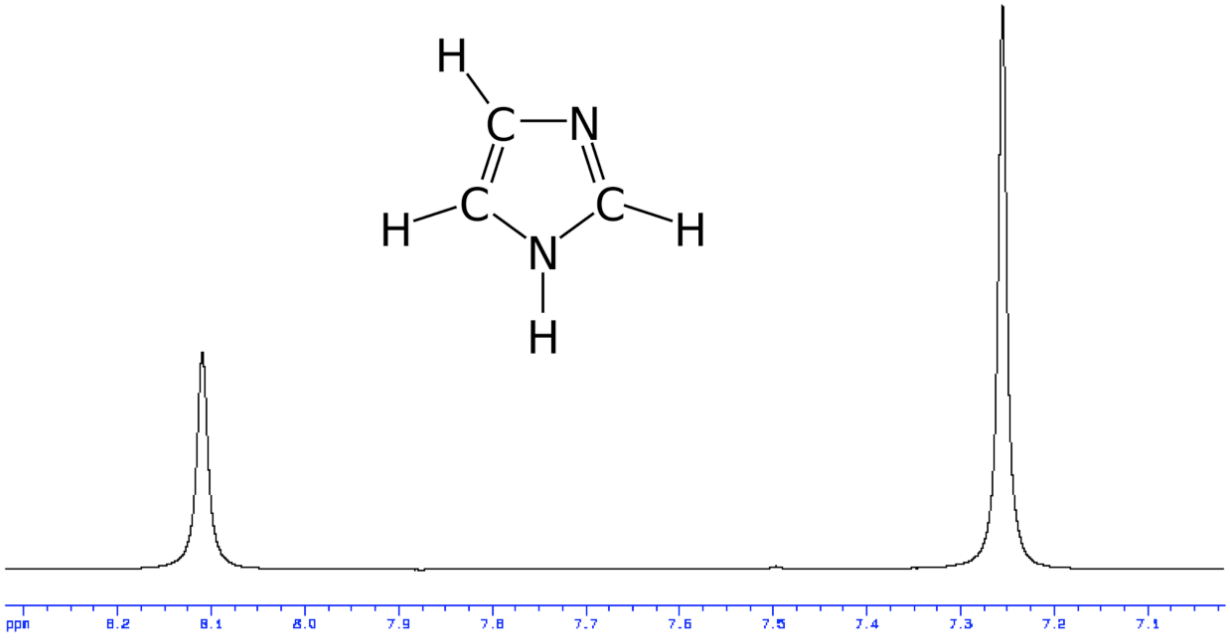

Figure 1.5: 1-D ^{1}H spectrum of the simple molecule imidazole taken from the Biological Magnetic Resonance Data Bank.The large peak results from the three protons bonded to carbon; the smaller peak is from the proton bonded to nitrogen.

Crucially, the different peaks indicate nuclei in different bond structures, but are not a direct spatial map of the molecule as in MRI. Spectra are further complicated by interactions such as dipolar coupling, direct interactions between spins, and through-bond coupling, interactions

mediated by the intervening electrons.

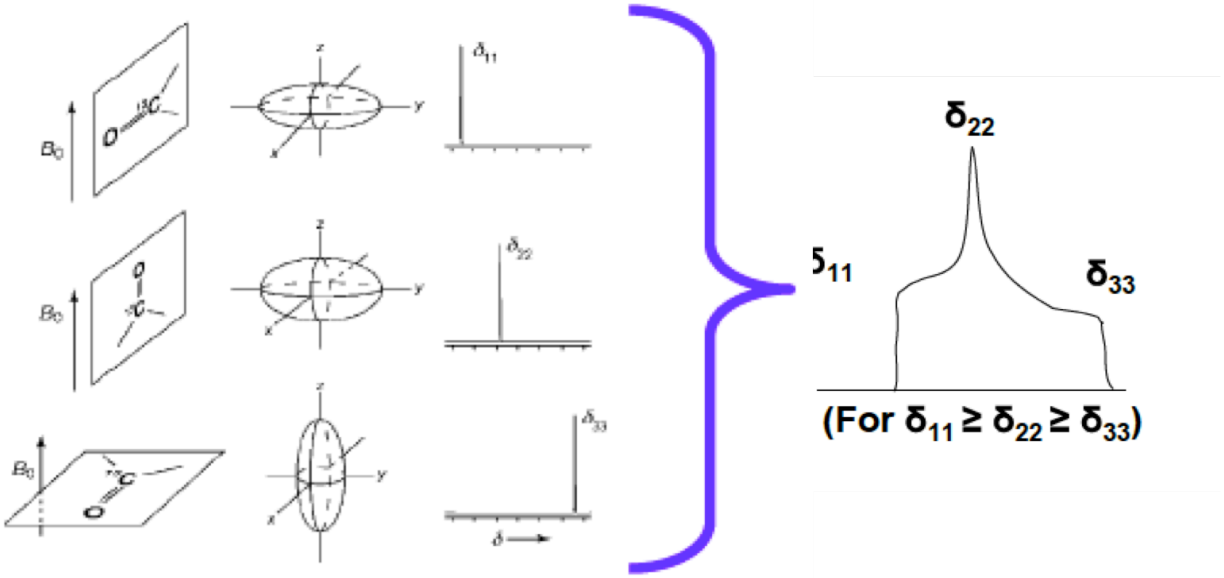

Figure 1.6: Characteristic "powder pattern" showing the anisotropic broadening seen in a solid sample taken from [2].

The symmetry of the beautiful narrow liquids peaks is broken by the anisotropy of aligned samples [16]. In solutions NMR, the effects of anisotropy and various spin-spin interactions are averaged out by the rapid tumbling of the molecules. Various techniques have been developed for solids NMR to deal with them.

The precession of the spins is detected via the current induced in a coil. The magnetic moment of the precessing spins is dwarfed by the magnitude of the external field used to induce their alignment. To detect the precession, the spins must be tilted such that their

field is orthogonal to the external field. This is accomplished by sending a current through the coil to generate a short rf pulse at the precession frequency of the spins. In the most basic NMR experiment, after a delay to allow the spins to reach equilibrium, a short "90-degree" rf pulse is used to tilt the spins into the x-y plane for detection.

1.3 NMR Instrumentation

The single largest instrument required for NMR is, of course, the magnet. The intense magnetic field needed to align the spins is generated by current flowing through a superconducting coil. This coil is immersed in liquid helium within a dewar. Around this is a dewar containing liquid nitrogen to reduce the boil-off rate of the helium. Smaller "shim" coils are used to adjust the magnetic field to compensate for any small inhomogeneities.

The gated rf pulses used in NMR experiments are generated within the console, the array of frequency generators and amplifiers. The returning signal is split and run through two pathways for quadrature detection to preserve the complex signal.

These rf pulses are mediated by the probe. The nuclei to be investigated, and the range of experiments possible, are greatly determined by the design of the probe. The probe contains the sample and the circuits needed to tune to each of the Larmor precession frequencies. It determines the physical condition of the sample during the experiment.

1.4 NMR Experiments

NMR experiments can be described by several different aspects–how the sample is physically held/manipulated, which nuclei are involved, and what rf pulses are used.

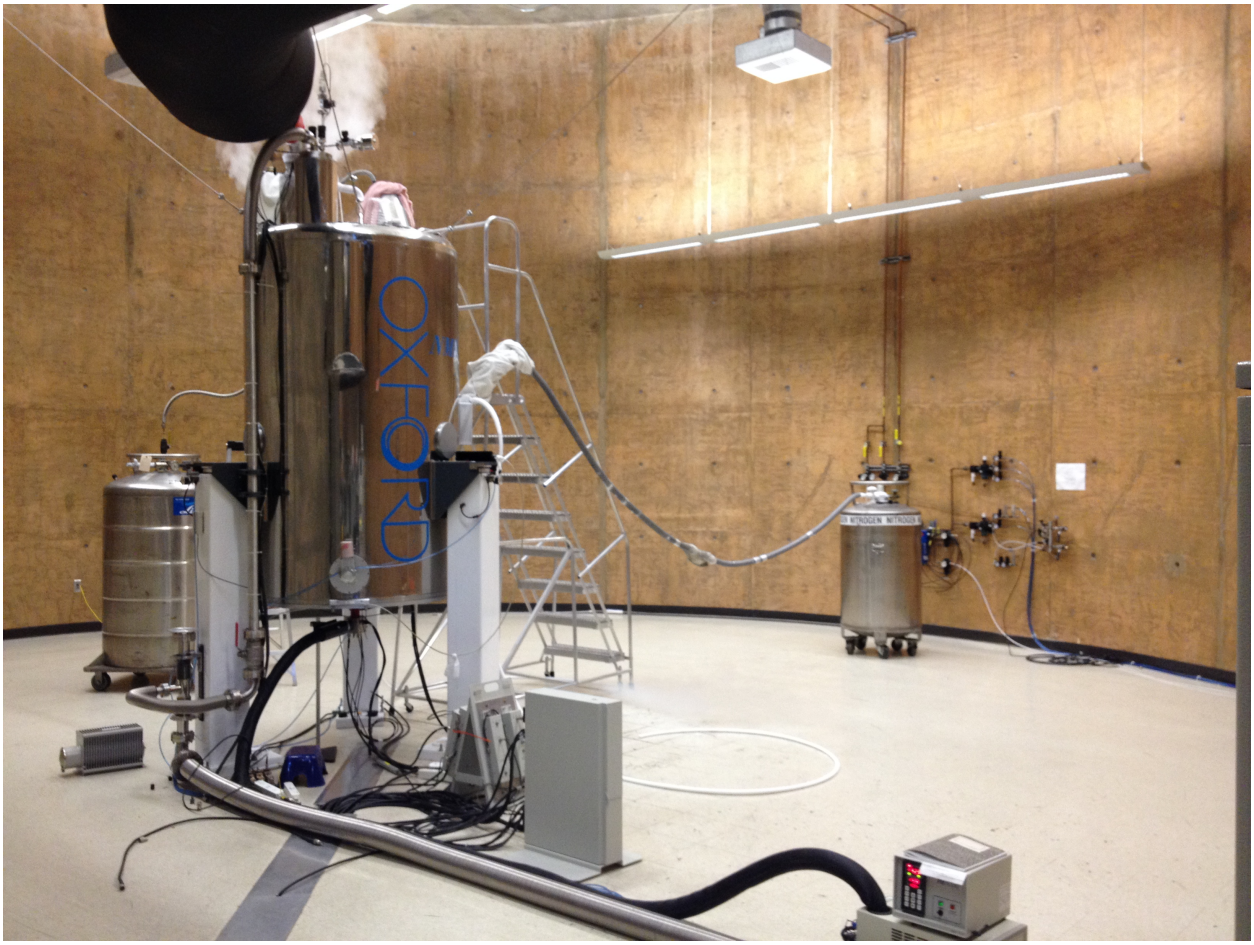

Figure 1.7: The 800 MHz magnetic in the Biological NMR Facility having its helium and nitrogen dewars topped off.

In the simplest experiment, a single rf pulse is used to tilt the spins from the z-axis into the x-y plane for detection.

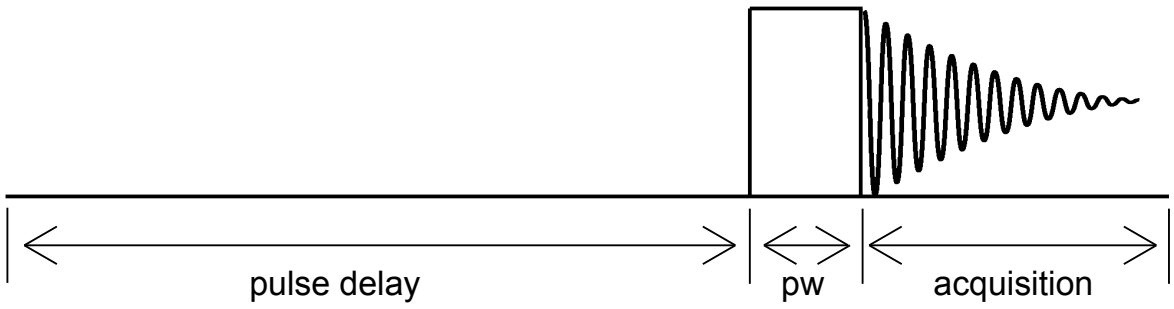

Figure 1.8: Pulse sequence diagram of the basic NMR experiment.

The initial delay period is required to allow the spins to return to equilibrium. The strength of the pulse is generally raised to the limit of what the hardware can handle. The length of the pulse is chosen to tilt the spins to the desired angle. At the given power level the pulse length is arrayed for calibration.

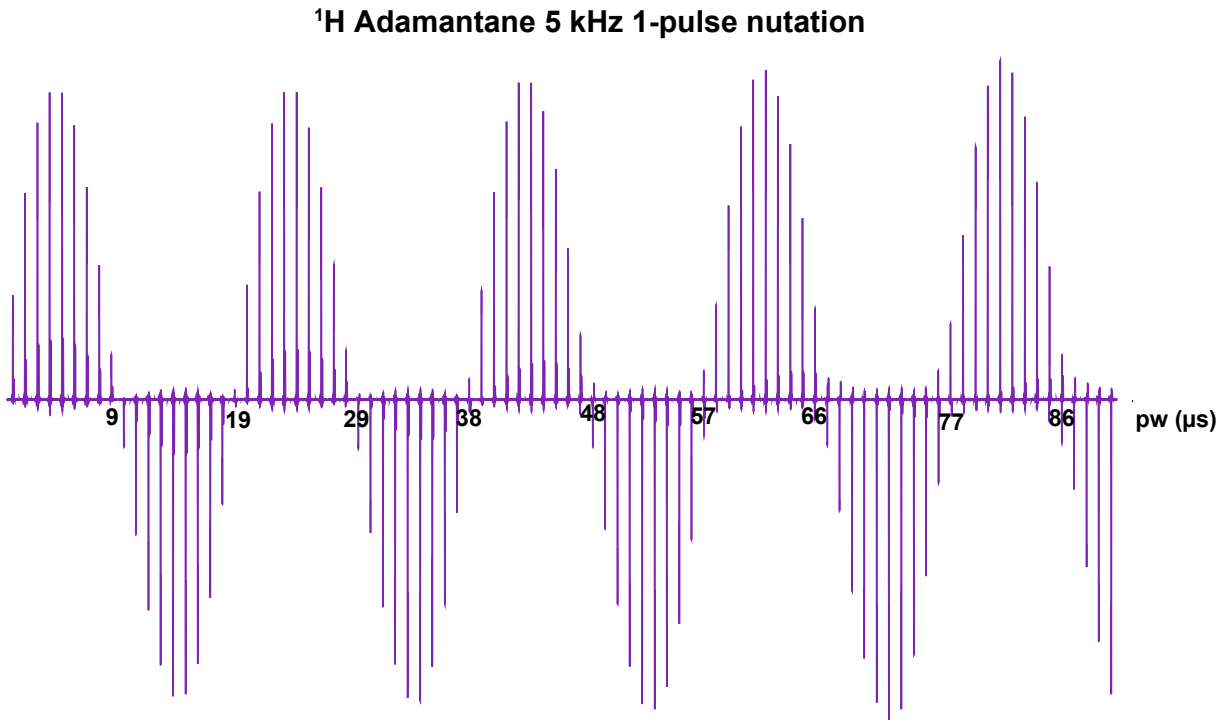

Figure 1.9: Nutation array generated by arraying the pulse width.

The pulse width is incremented by 1μs in each step; the rotation of the magnetic moment can be seen when the spectra are lined up. The first maximum occurs when the moment has been tilted along the y-axis; this pulse length is the "90-time", since the moment has been rotated by 90°.

One of the most important techniques of solid-state NMR is purely mechanical–the sample is placed in a rotor that is spun rapidly at the "magic angle"[17] of 54.74°. This averages out broadening from anisotropy and through-space interactions such as dipolar coupling [18]. Mechanically this angle can be seen as the diagonal of a cube. Mathematically it is the angle at which the second-order Legendre polynomial goes to zero.

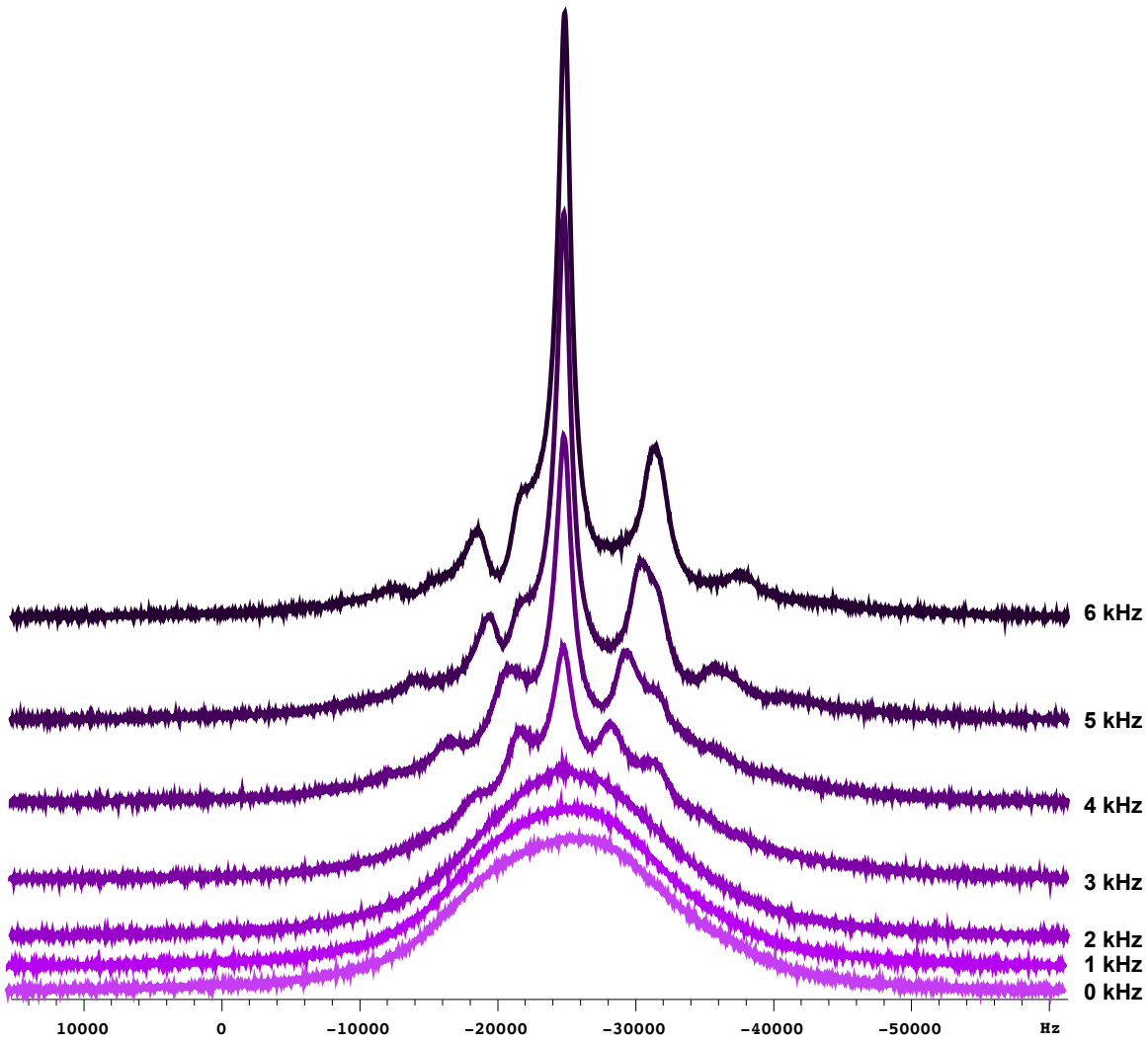

Figure 1.10: Sharpening of the ^{1}H signal detected on adamantane as the rotor is spun up from 0 kHz to 7 kHz.

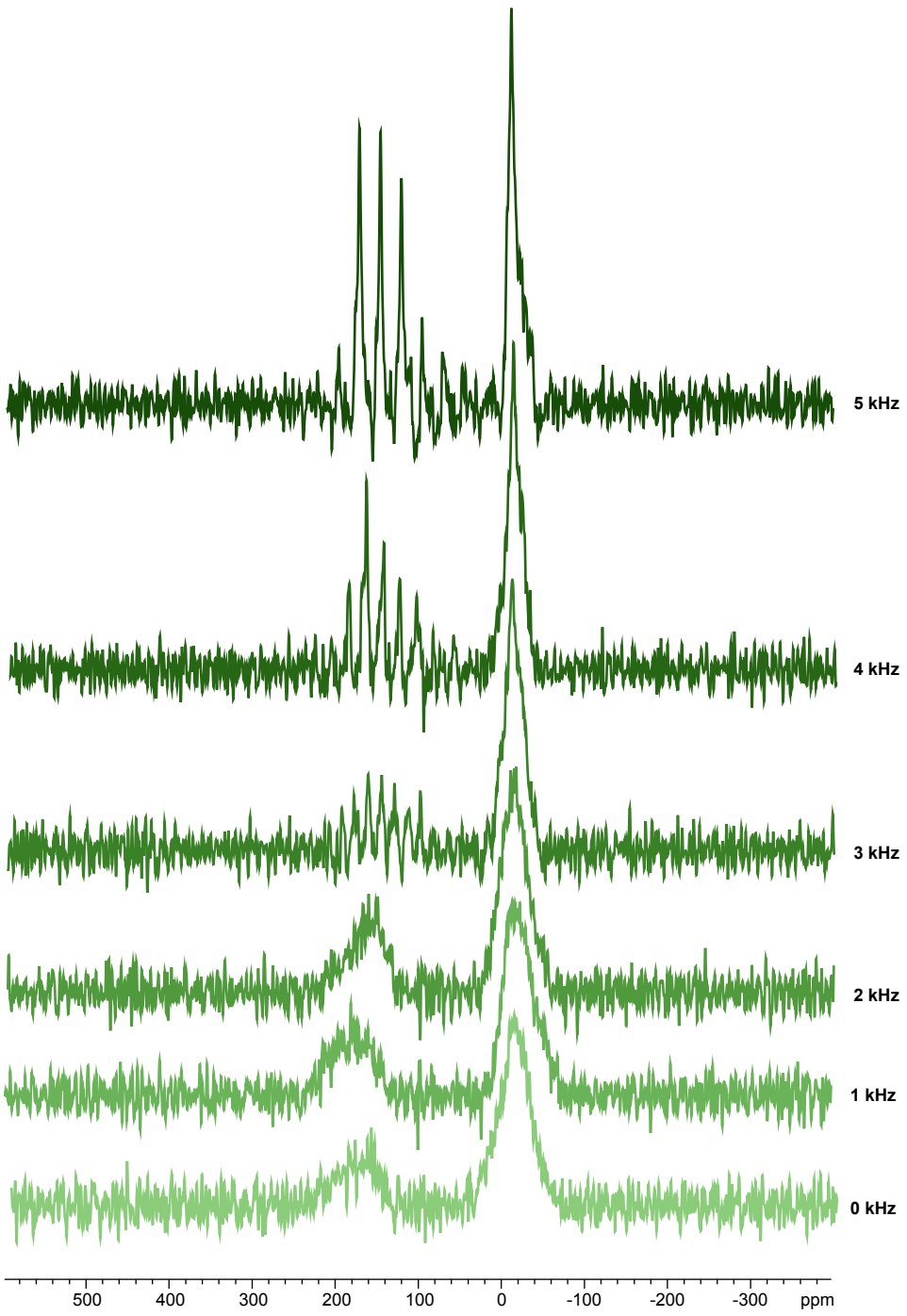

Figure 1.11: Sharpening of the ^{13}C signal detected on alanine as the rotor is spun up from 0 kHz to 6 kHz.

The resultant narrowing of the peaks makes detection easier and reduces the overlap of peaks

on complicated spectra.

In cross-polarization, simultaneous rf pulses at two frequencies are used to bring two nuclear spin species into thermodynamic equilibrium, allowing magnetization to be transferred from a high-abundance, high gamma nuclei such as proton to rarer spins [19]. In low-power decoupling, long rf pulses are used to, by keeping spins rotating, prevent homonuclear dipolar coupling, especially between proton spins. Combining CP and decoupling allows the detection of rare, low-gamma nuclei [20].

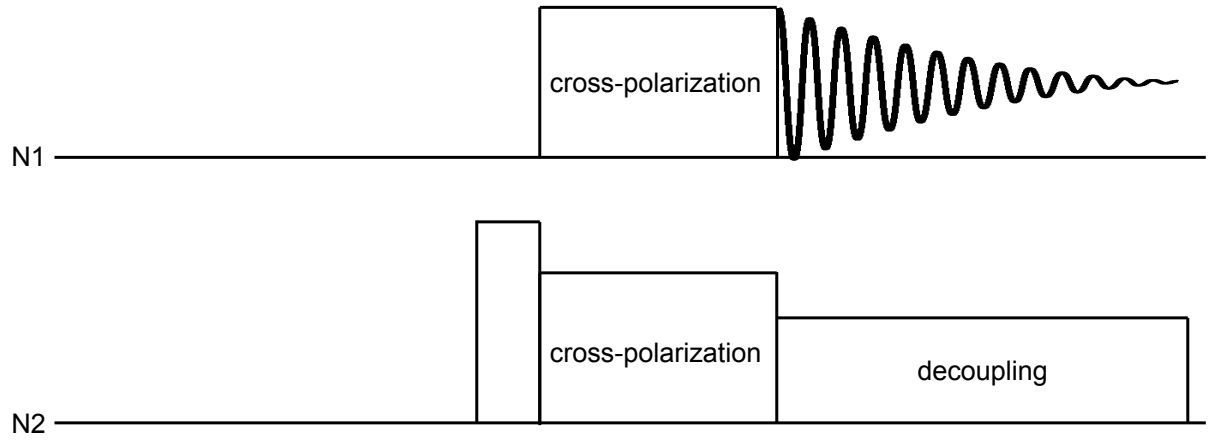

Figure 1.12: Pulse sequence diagram of a basic cross-polarization experiment with low-power decoupling.

Each level of the diagram indicates a different nucleus. The top level is the nucleus whose signal will be detected at the end of the experiment. This sequence begins with a 90-pulse on the higher-gamma spins. Simultaneous pulses on two channels are then used to create the matching conditions necessary for cross-polarization to occur. This leads to a significant improvement in signal-to-noise.

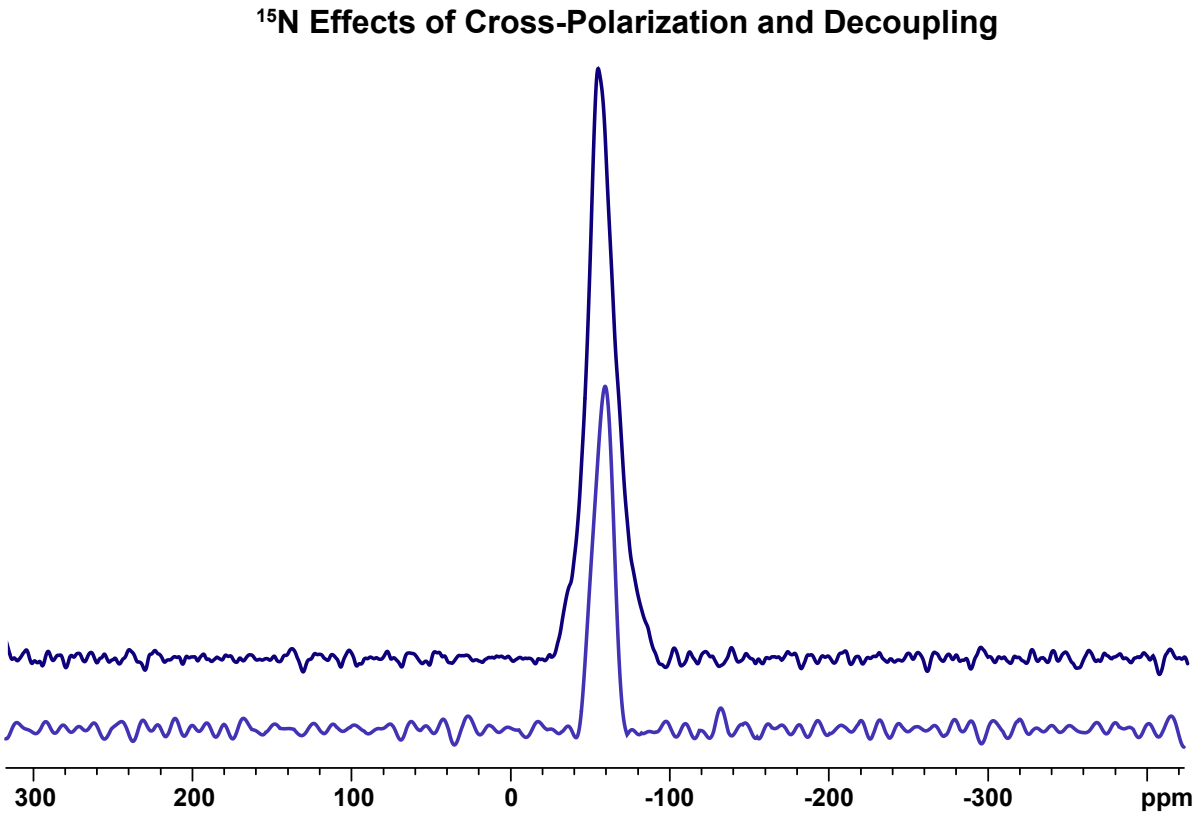

Figure 1.13: The improvement in signal from a cross-polarization and decoupling sequence compared to the basic one-pulse sequence.

An additional rf pulse can be added on the first channel at the end of the sequence to tilt the magnetization as desired before detection.

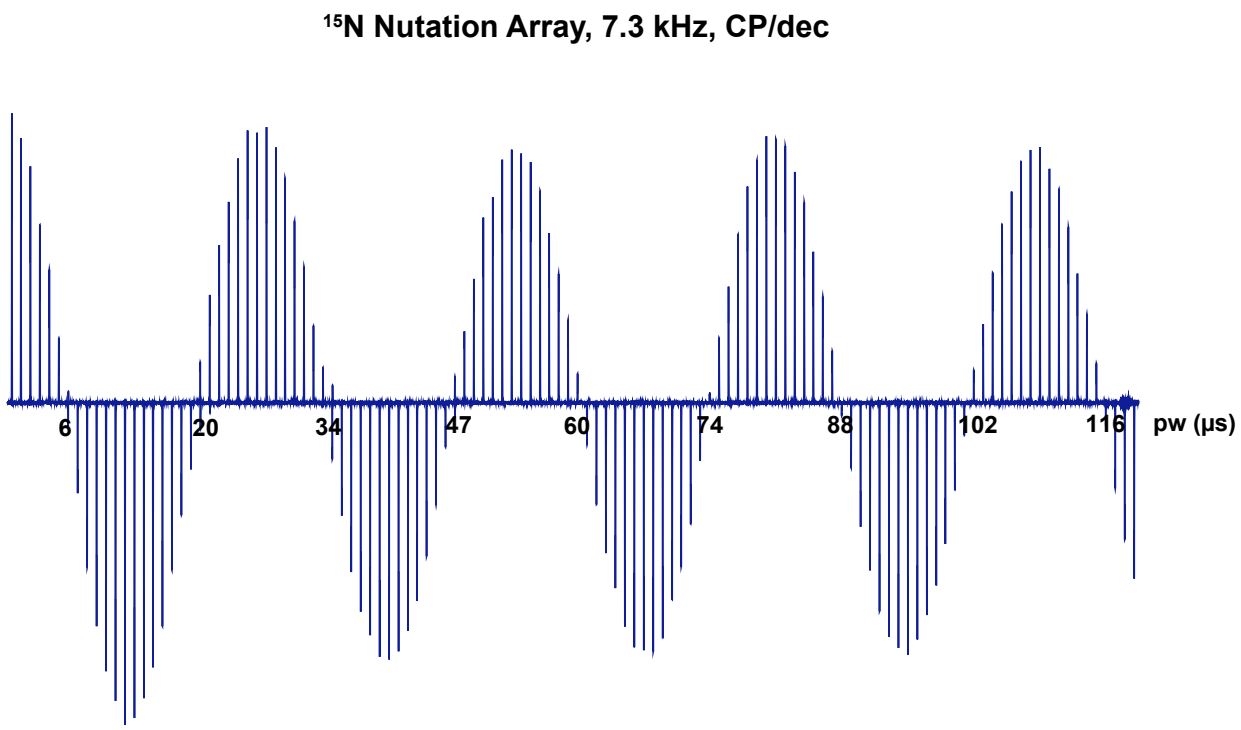

Figure 1.14: The pw array in a cross-polarization/decoupling sequence.

When this pw is arrayed, unlike in the one-pulse case, the magnetic moment begins at the maximum, given the magnetization transfer, and goes down from there.

Both cross-polarization and decoupling are techniques for experiments in which multiple species of nuclei are studied. Pulse sequences can be used to transfer magnetization either through space or through electron bonds, yielding the distance and angular constraints, matched to the bond structure, needed to solve the structure of complex molecules [21, 22, 23].

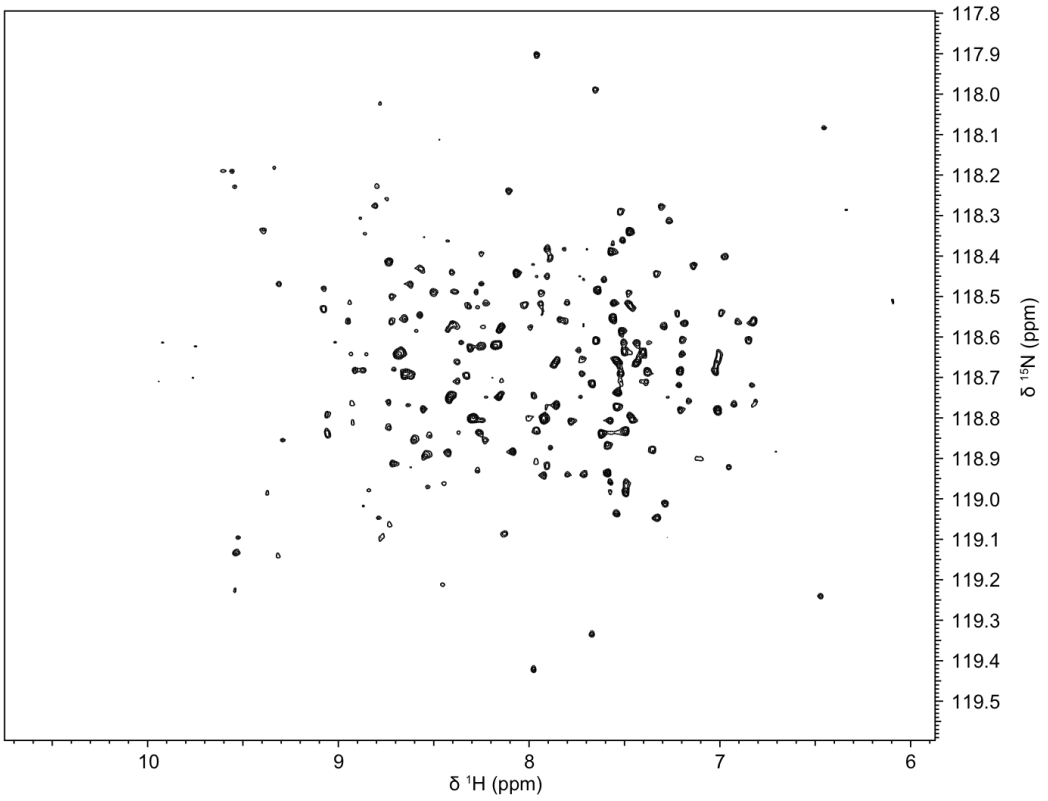

Figure 1.15: Two-dimensional spectrum showing the correlations between ^{15}N and ^{1}H nuclei.

This information can also be used to study the change in structure resulting from the binding of molecules by looking at the shift in peaks.

Deuteration of biomacromolecules is commonly used to reduce homonuclear dipolar coupling between the abundant, high-gamma proton spins [24, 25, 26]. This reduction in the strength of dipolar coupling means that low-power decoupling can be used even at moderate MAS frequencies [27, 28, 29]. This deuteration is, however, quite expensive; even so deuterium is not commonly used for direct detection in NMR. Each nuclei that is to be detected requires its own circuit in the probe, and very few commercial probes are available with a dedicated deuterium channel. Given the cost of deuterated samples, ideally as much use as possible

would be made of these nuclei! And aside from adding another dimension to the experiments possible, deuterium, as a spin-1 nucleus, is quadrupolar. The spectra display charactersitic splittings, the separation of which serves as an indication of the mobility of the sample [30, 31, 32, 33]. Deuterium also has a very short delay time, the time required for the spins to return to equilibrium after an rf pulse, allwoing experiments to be performed relatively quickly. Cross-polarization allows this short delay time to be used for other nuclei.

Chapter 2

The Probe Design

2.1 NMR probe fundamentals

An NMR probe is fundamentally a collection of LC circuits tuned to resonate at the Larmor precession frequencies of the nuclei of interest. Each type of nucleus requires its own circuit, referred to as a channel. The inductance of the circuit is determined by the coil into which the sample is inserted. Variable capacitances are used to tune the circuit to the desired frequency and to match the impedance to the voltage source. The primary engineering difficulties lay in designing components that can handle high rf power and in fitting all of the necessary components into the narrow bore of the magnet.

2.2 The Choice of Frequencies

NMR probes are generally designed with two or three channels sharing a signal coil to maximize the range of experiments possible, as multidimensional NMR requires a dedicated channel for each nuclei. More channels allow more complex experiments, but the small

sample size and orthogonality requirement generally limits a probe to no more than two sample coils. The spatial constraints imposed by the magnet limit how many channels can fit in the bore; additionally, the difficulty of designing the isolation required increases significantly with each channel added to a signal coil.

The composition of amino acids means that biological NMR is generally done with $^{1}H/^{13}C/^{15}N$ probe circuits.

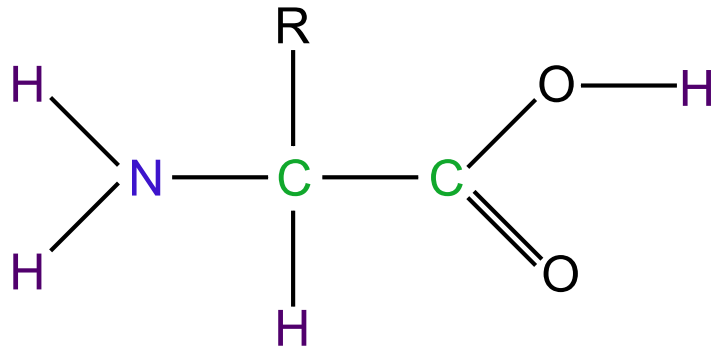

Figure 2.1: The structure of an amino acid with generic functional group R.

Both proton and flourine are high-gamma nuclei ideal for transferring magnetization to the lower-gamma carbon and nitrogen through cross-polarization. Any probe circuit for biological NMR is likely to include a high-gamma channel.

2.3 NMR Coils

The design of an NMR probe begins with the selection of the coil(s) to be used based on the sample systems of interest.

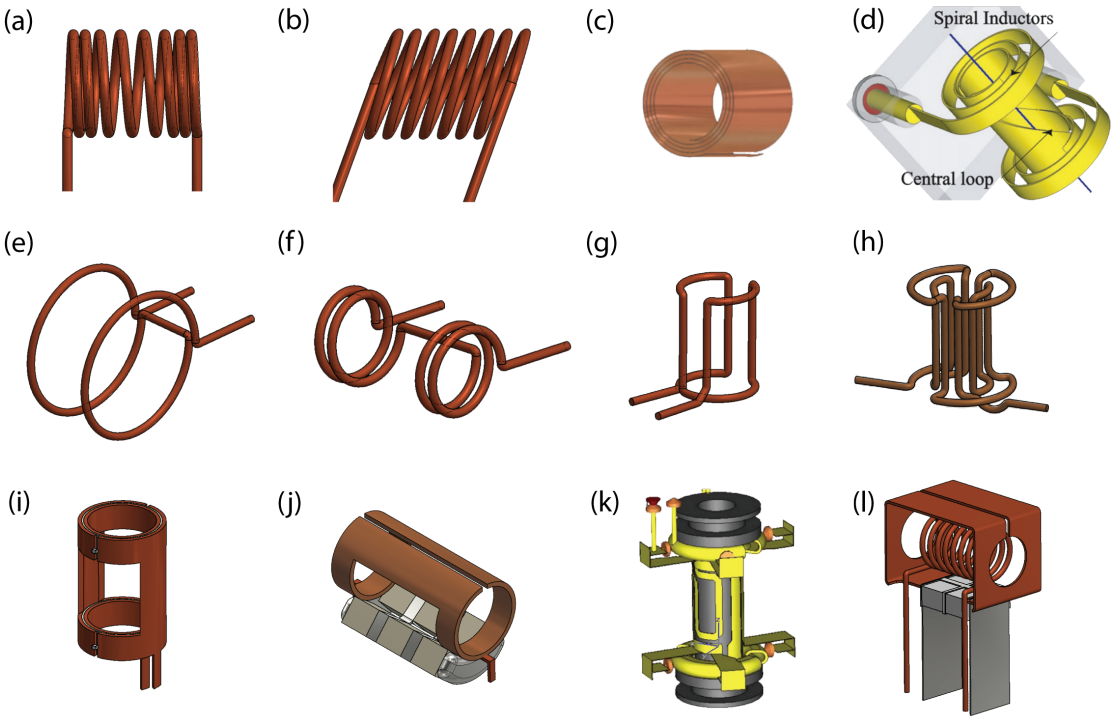

Figure 2.2: The wide array of coils used in solid-state NMR probes: a, b, l solenoidal; c, d scroll coils; e, f, Helmholtz arrays; g, h, saddle coils; i, j slotted-tube resonators.

A selection of coils available is shown in Fig. 2.2. Solenoids are commonly used; they are relatively easy to wind and have a high signal-to-noise factor. Slotted-tube resonators have a lower signal-to-noise ratio, as they are a one-turn coil, but can sustain a high voltage for long periods without significant heating of the sample [34, 35, 36]. Saddle coils are far more difficult to wind than a solenoid, and don't have quite as high a signal-to-noise, but produce a field that is orthogonal to B_0 at any sample angle [37].

Signal coils can be wound by hand from wire, machined from tubing with lathe and endmill, or printed on sheets and wound about a form. Two coils with orthogonal B_1 fields can be

placed coaxially without interference, allowing for a bit of diversification. Using two coils also reduces the isolation required as fewer channels are on the same circuit. A coaxial arrangment is shown in Fig. 2.2l.

2.4 The Selected Coils

Given that this probe was from its inception intended to have four channels, and to be used to study delicate biological molecules, the decision was made to use a coaxial arrangement with two coils [38, 39, 40].

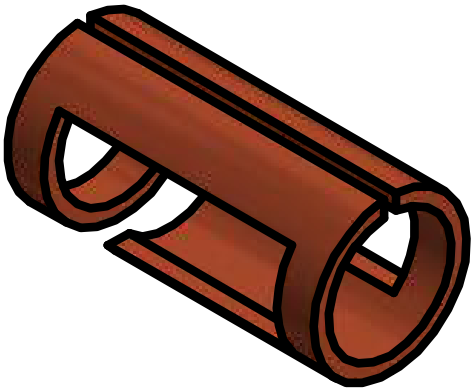

(a) Original slotted-tube resonator.

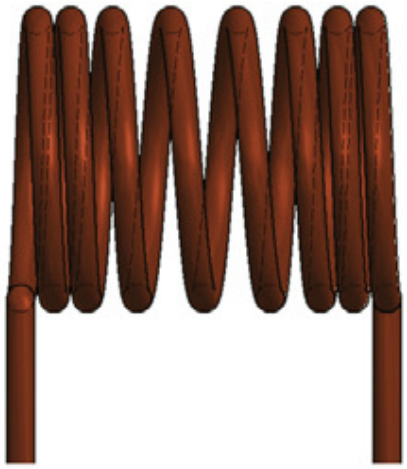

(b) Variable-pitch solenoid.

Figure 2.3: The two original coils.

The outer coil was to be an slotted-tube resonator for the proton circuit; the proton channel is designed to be used for decoupling and cross-polarization, not direct detection, so minimizing electric heating of the sample [41] is more important than signal-to-noise. The resonator was machined by hand on lathe and mill in the student machine shop from OFHC copper tubing.

The three lower-gamma nuclei are then on a variable-pitch solenoid to maximize the signal-to-noise for direct detection [42, 43]. The solenoid was wound by hand from "magic" wire, OFHC copper coated with palladium to have an overall magnetic susceptibility of zero.

The initial slotted-tube resonator proved too inefficient to even allow for the desired cross-polarization and decoupling, so the decision was made to instead utilize a modified Alderman-Grant coil [44].

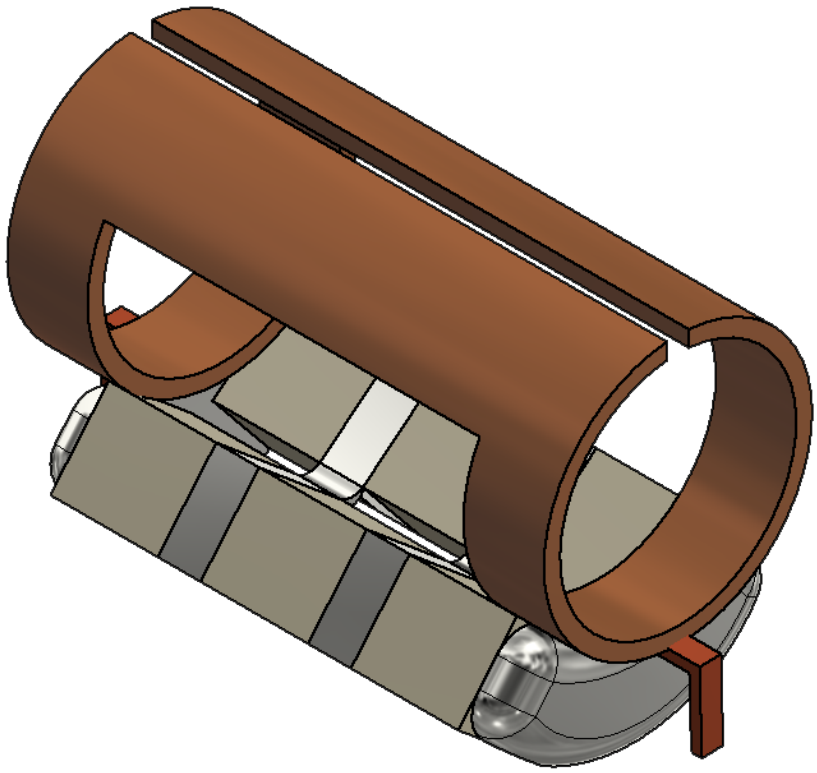

Figure 2.4: The modified Alderman-Grant coil with curved capacitive bridge.

The blank for the coil was again machined from copper tubing; the fun came in attempting

to solder the bridge of tiny chip capacitors in place.

Figure 2.5: The blank for the MAG resonator with a penny for scale.

A long and painful process of trial and error and dodging ricocheting super hot projectiles proved that the most effective approach was machining a holder with a depression for the bridge that fit within the coil blank from teflon, delicately coating the chips capacitors with solder paste, and then blasting them with a heat gun. Anything involving clamps or tension ended in ricochets and angry labmates.

2.5 NMR Probe Circuits

An NMR probe is a set of LC circuits each tuned such that its resonant frequency is that of the Larmor precession frequency of a specific nucleus.

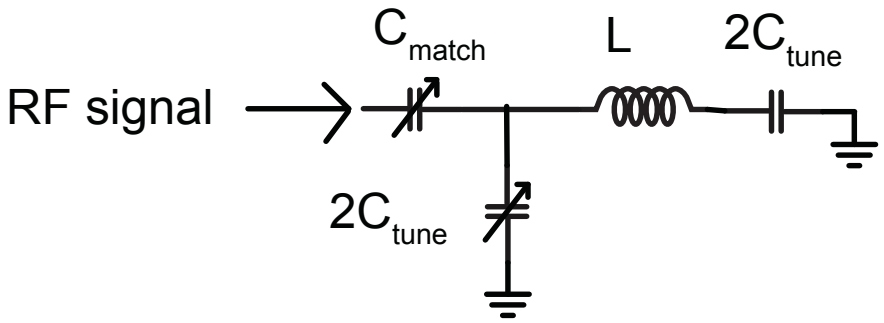

Figure 2.6: A basic NMR probe circuit with a single channel. The inductance L results from the signal coil, the circuit is impedance matched by adjusting the variable capacitance C_{match}, and the response frequency is adjusted by variable capacitance C_{tune} which is split across the coil to balance the voltage.

The most basic probe consists of the inductive signal coil, variable capacitances to allow the probe to be tuned and matched to the impedance of the voltage source, and an additional capacitance to ground across the coil from the channel to balance the reactances across the coil, preventing a voltage node in the center of the coil [45, 40].

The circuit resonates at $f = \frac{1}{\sqrt{LC}}$.

As more channels are added the circuit becomes more complicated with the addition of isolation elements to control the paths of each rf frequency[46].

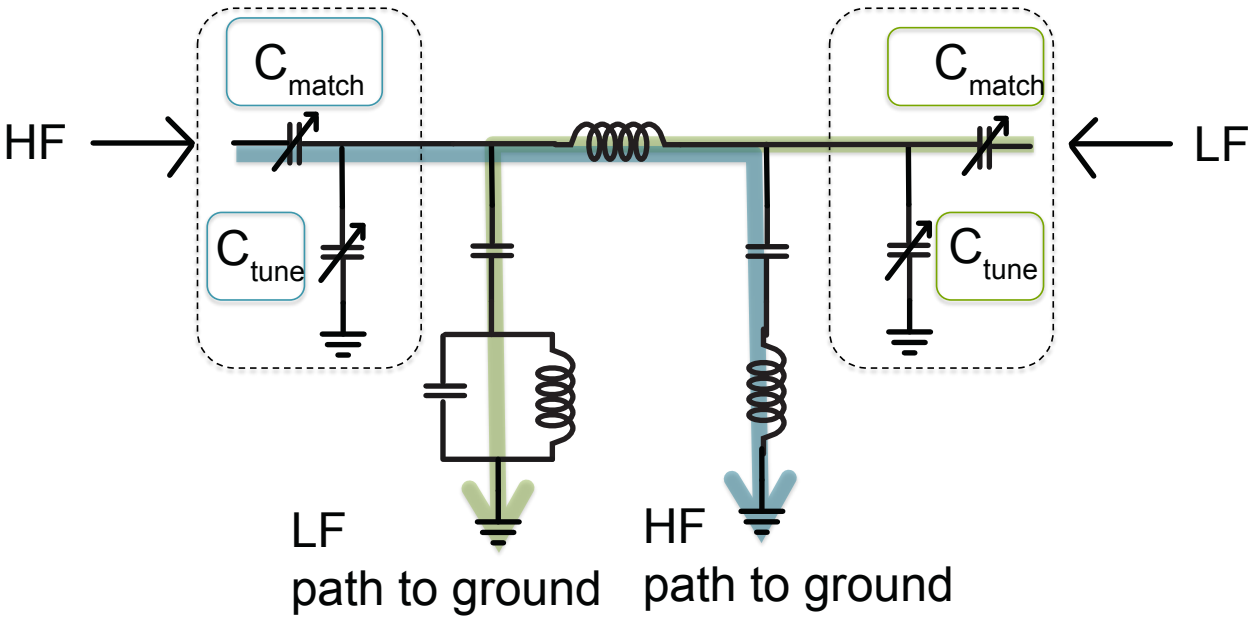

Figure 2.7: A somewhat more complicated NMR probe circuit with two channels and isolation elements. The inductance is set by the signal coil; each channel contains variable capacitances for tune and match. High and low frequency paths to ground, made of capacitive and inductive elements, are used to control the paths of each signal frequency.

Each channel still contains the two variable capacitances needed to tune and match that sub-circuit.

The question, then, is how to construct these circuit elements. Commercial chip capacitors are very modular and can be easily switched out; using chip capacitor boards allows the tuning frequency of each channel to be adjusted quickly. However, they cannot handle high power levels [47, 48].

Transmission line segments reactances are a function of length relative to the wavelength of the propagating signal, a useful dependence for high-frequency rf engineering [49].

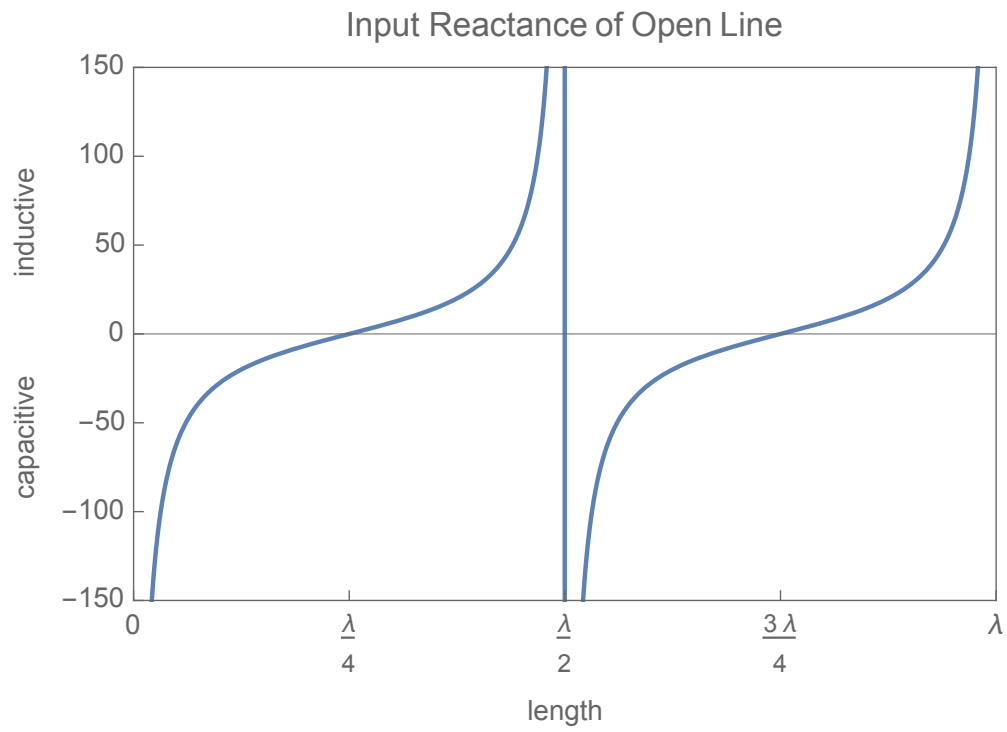

(a) Reactance of open transmission line.

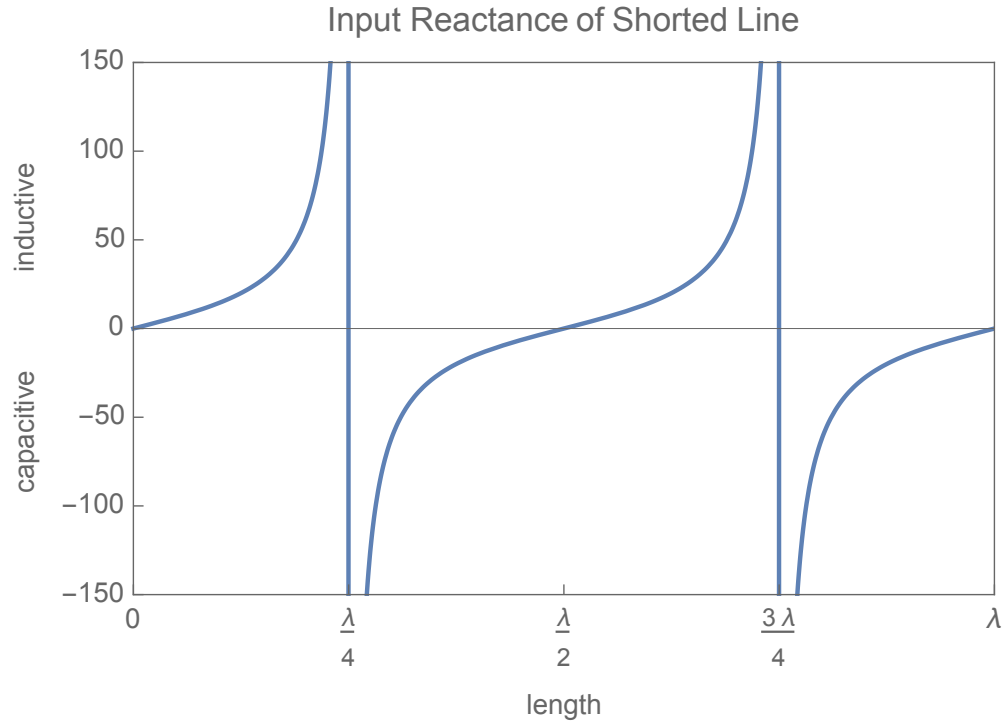

(b) Reactance of shorted transmission line.

Figure 2.8: The reactances of open and shorted transmission line segments as a function of length relative to wavelength of transmitted signal. At high rf frequencies quarter-wavelength transmission line segments can be used as isolation elements, in addition to the normal capacitive and inductive properties.

These segments can be used as capacitive, inductive, and isolation elements in NMR probe circuits [50, 51].

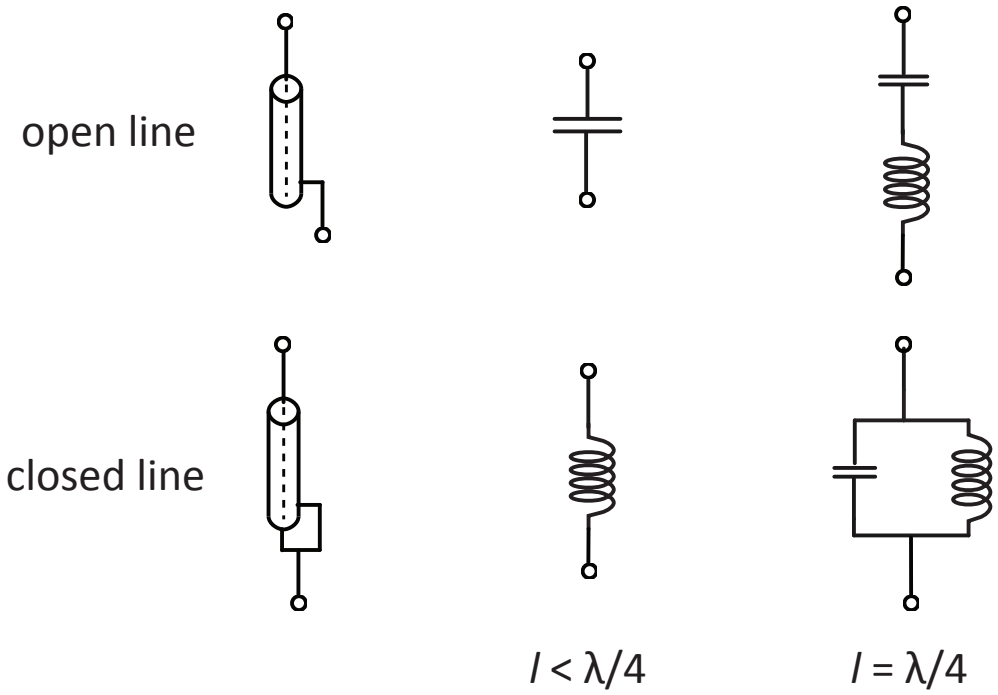

Figure 2.9: A diagram showing the transmission line segments used in probe construction and the equivalent discrete circuit elements.

They are robust, able to handle high power levels, and their cylindrical symmetry lends itself to fitting multiple circuits into the narrow bore of the magnet. They can also be machined on the generation of equipment available in the student machine shop, a definite advantage for turn-around time.

2.6 Circuit Design

Each of the coaxial coils has its own rf circuit to allow the channels to be tuned and prevent interference between the channels.

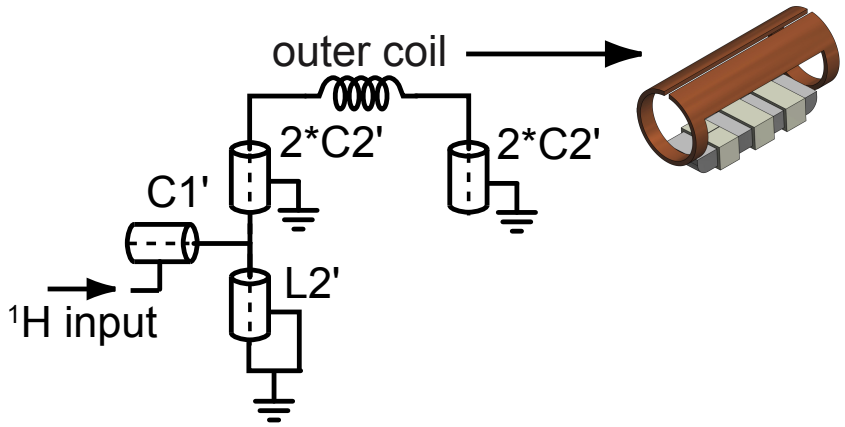

Figure 2.10: The circuit of the modified Alderman-Grant coil in transmission line notation.

The variable capacitances C1' and C2' are required to match the circuit to the input load and tune the resonant frequency to the Larmor precession frequency of ^{1}H. The tune capacitance of the modified Alderman-Grant resonator C2' is split over the coil to balance the voltage [45, 40]. The match capacitance C1', being an order of magnitude smaller, does not have to be split. The additional inductive element L2' is required to tune the circuit to the high frequency of the proton signal. Without the additional inductance the dimensions of the transmission line segments required would be prohibitively small; machining them by hand would be an incredibly difficult task, and more importantly, there would be almost no adjustment range and a strong enough temperature dependence that the channel could not even be tuned for the length of an experiment.

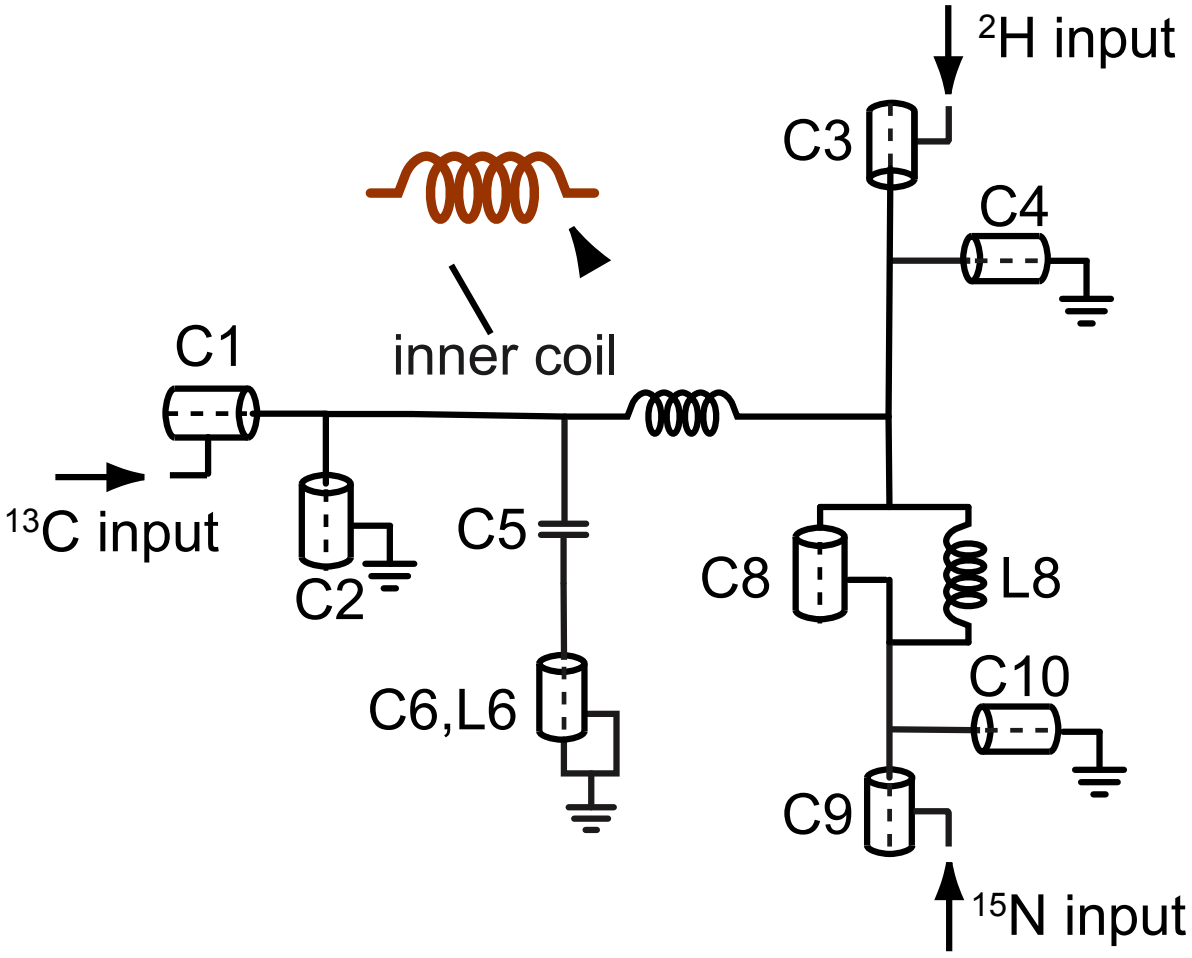

Figure 2.11: The circuit of the solenoid coil in transmission line notation.

The solenoid circuit has the tune (C2, C4, and C10) and match (C1, C3, C9) capacitances required for each resonance frequency. The additional elements are required for isolation between the different frequencies. Together C5, C6, and L6 act as a low-frequency path to ground, with values chosen such that $C5 = \frac{\omega_{13C}^2 - \omega_{2H}^2}{L_6 \omega_{13C}^2 \omega_{2H}^2}$, where ω_{13C}^2 is the Larmor precession frequency of ^{13}C and ω_{2H}^2 is the Larmor precession frequency of ^{2}H. The pair C8 and L8 act as a high frequency block [52, 53].

2.7 Mechanical Design

As mentioned previously, the design of the probe begins with the choice of signal coil(s). It is through these coils that every interaction with the sample is mediated. The sample is contained within a rotor placed within these coils. To stabilize this arrangement, the coils are contained within a stator purchased from Revolution NMR.

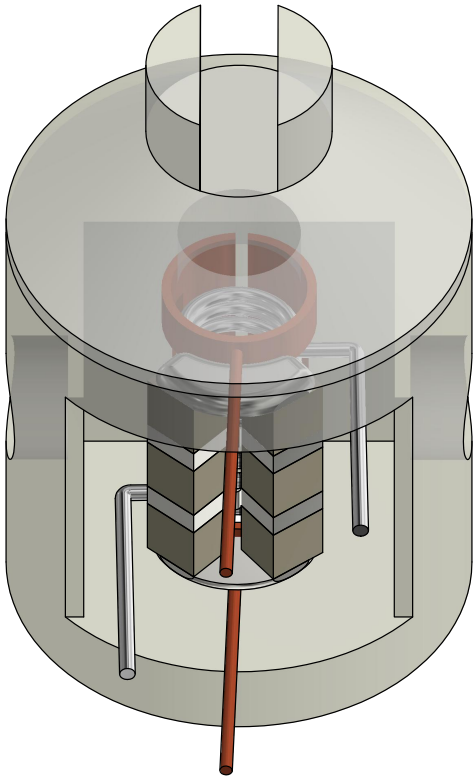

(a) Angled back view of the stator.

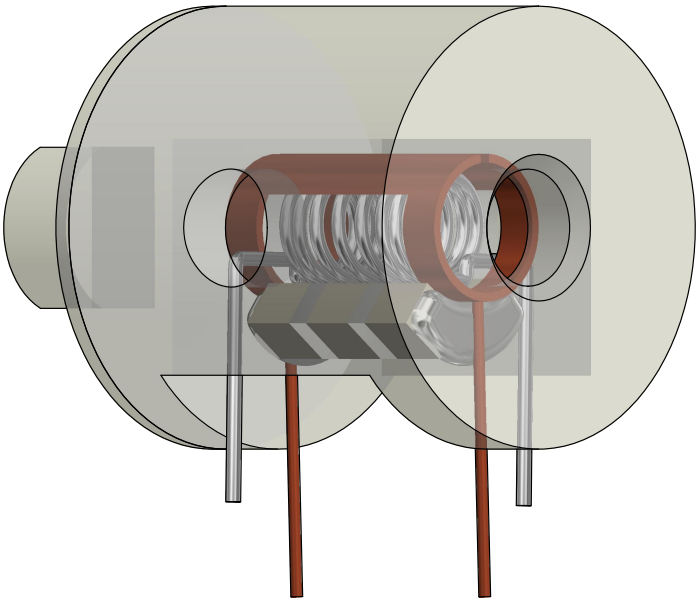

(b) Angled side view of the stator.

Figure 2.12: Two views of the stator and coaxial coils. The back view shows the attachment for the magic angle adjust on the back cap and the central cavity in which the coils are placed. The side view shows the front opening where the sample rotor is inserted and the side opening through which the bearing air is directed.

Pathways cut within the stator direct the flow of the bearing and drive air to cause the rapid spinning of the rotor in which the sample is contained.

The rear cap of the stator is then connected to a threaded rod that runs through the top plate of the probe, allowing precise control of the angle at which the rotor is spun.

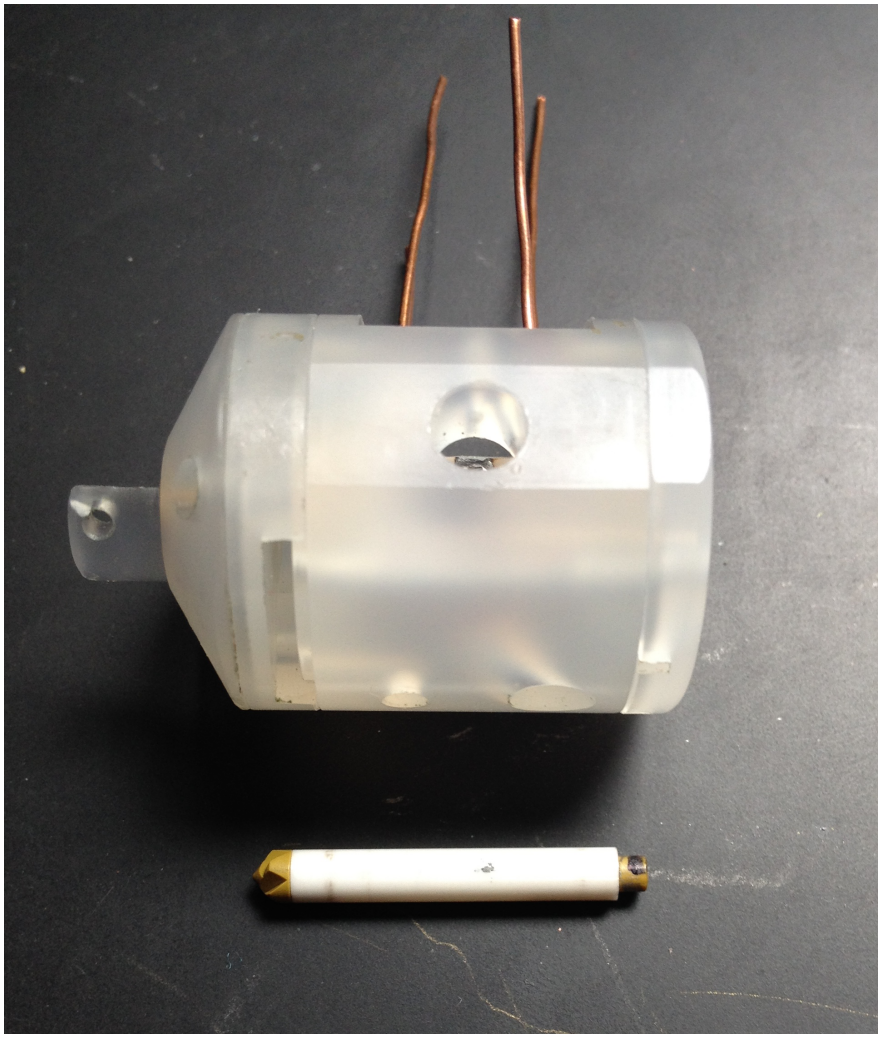

Figure 2.13: A picture of a sample rotor next to the stator. The black marking on the rear cap is used to help the fiberoptic system used to measure the spinning speed by reflecting light from the cap.

The entire probe circuit and the hardware required to spin the sample rotor, measure the spinning speed, and control the temperature must all fit within the 2-inch bore of the magnet.

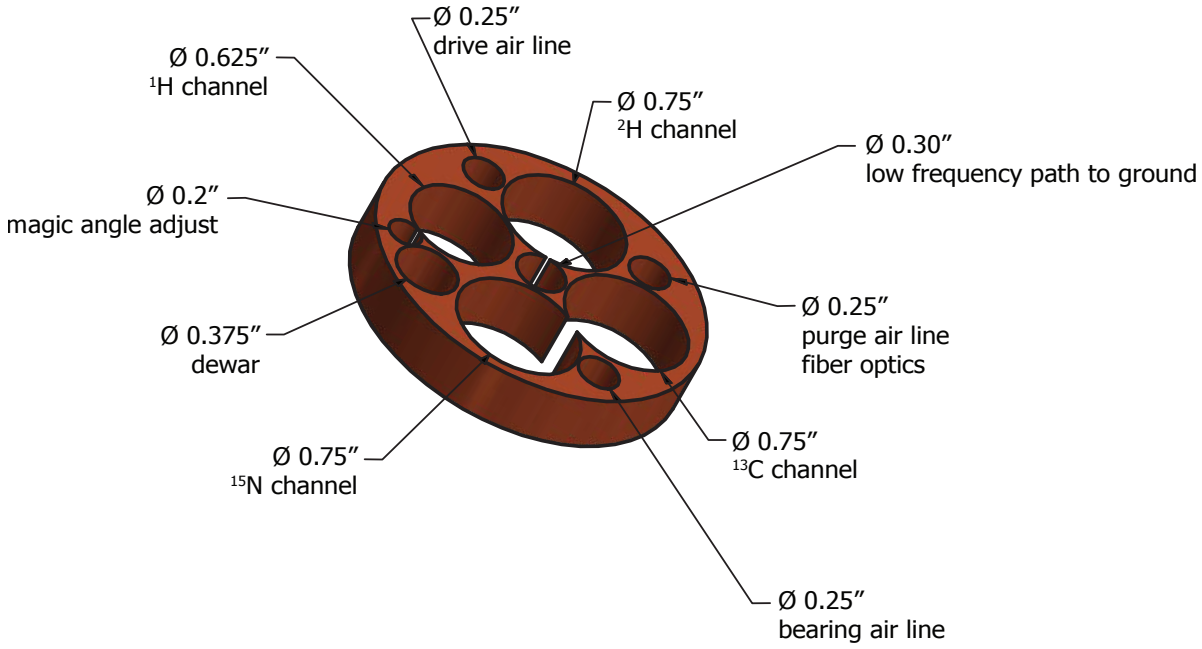

Figure 2.14: Schematic of the top plate of the probe frame.

The bulk of the available room is of course taken by the four channels, with the air lines and other necessary connections scattered in the remaining gaps. The entire assembly is contained within an aluminum can for protection and structural support, to prevent anything being caught in the magnet bore, and to help keep the air lines where they belong.

As one might expect, this makes for a very dense assembly, with little room to spare. Preventing the different coil leads from accidentally touching adds an extra layer of fun to the assembly process.

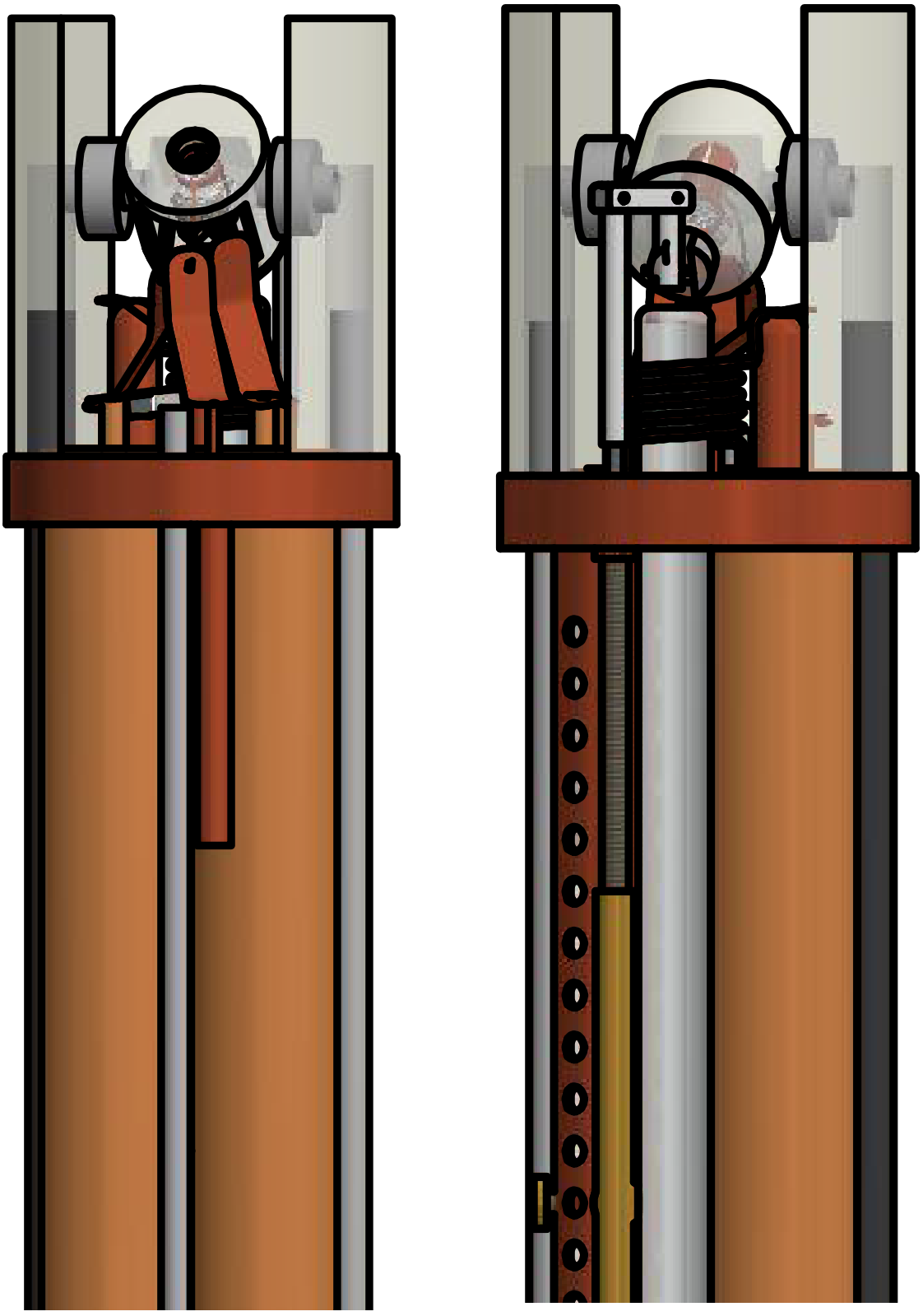

(a) Front view of the probehead.

(b) Back view of the probehead.

Figure 2.15: The tight arrangement of components necessitated by the magnet bore diameter.

The cylindrical symmetry of the transmission line segments allows each channel to be contained within an outer ground plane such that the cylinders can be in contact. It would otherwise be impossible to fit this many components in the magnet!

Shown in Fig. 2.16 is a diagram of the assembled components of the ^{13}C channel [51]. Each channel is composed of a multitude of conductive and dielectric parts to make the circuit, plus the necessary structural supports and componenets to allow for adjustment.

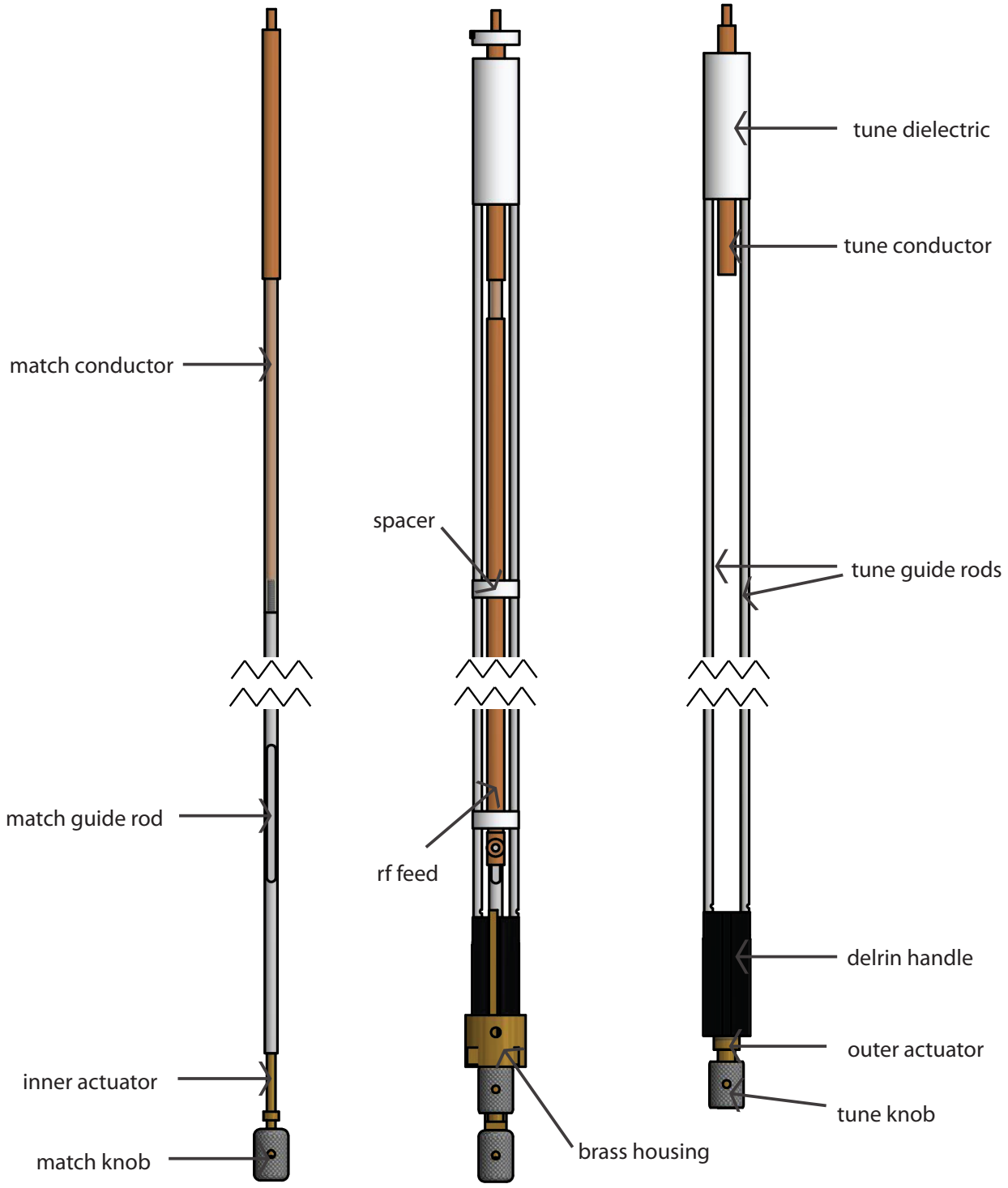

Figure 2.16: In the center is a front view schematic of the assembled components of the ^{13}C channel; shown to the left and right are the tune and match components in isolation to more clearly illustrate their composition. The length of the diagram has been truncated for clarity. The variable match capacitance is achieved by adjusting the depth of insertion of the central match conducter within the top piece, while the variable tune conductance is controlled by moving the dielectric between the top piece and the outer ground plane. The match conducter is capacitively coupled to the rf feed rod.

component	^{13}C	^{2}H	^{15}N
match guide rod (L)	15”	17”	18.5”
tune guide rods (L)	20”	18.5”	20.5”
rf feed (L)	17.5”	16.5”	19.5”
tune dielectric (L)	2.125”	2”	3”
tune dielectric (ID)	0.25”	0.45”	0.43”
lower match conductor (L)	4.75”	4.75”	4”
upper match conductor (L)	2.25”	1.125”	2.5”
upper match conductor (OD)	0.125”	0.185”	0.25”
tune conductor (L)	3.625”	3.825”	1.75”
tune conductor (OD)	0.25”	0.435”	0.435”
tune conductor (ID)	0.2”	0.375”	.325”

Table 2.1: Heteronuclear channel dimensions.

The nested cylindrical components of the design minimize the required cross-sectional area of each channel. All of the components, except for the brass assembly pieces that hold the components in the outer cylinder, were machined by hand in the student machine shop.

The dimensions of the components for each of the heteronuclear channels are given in Table 2.1 below. The match guide rods are machined from Delrin with an outer diameter of 3/16” and the tune guide rods from Delrin with an outer diameter of 0.125”.

The proton channel is contained within a narrower cylinder and has a slightly different design, containing an additional inductive element to allow tuning at high frequency [51].

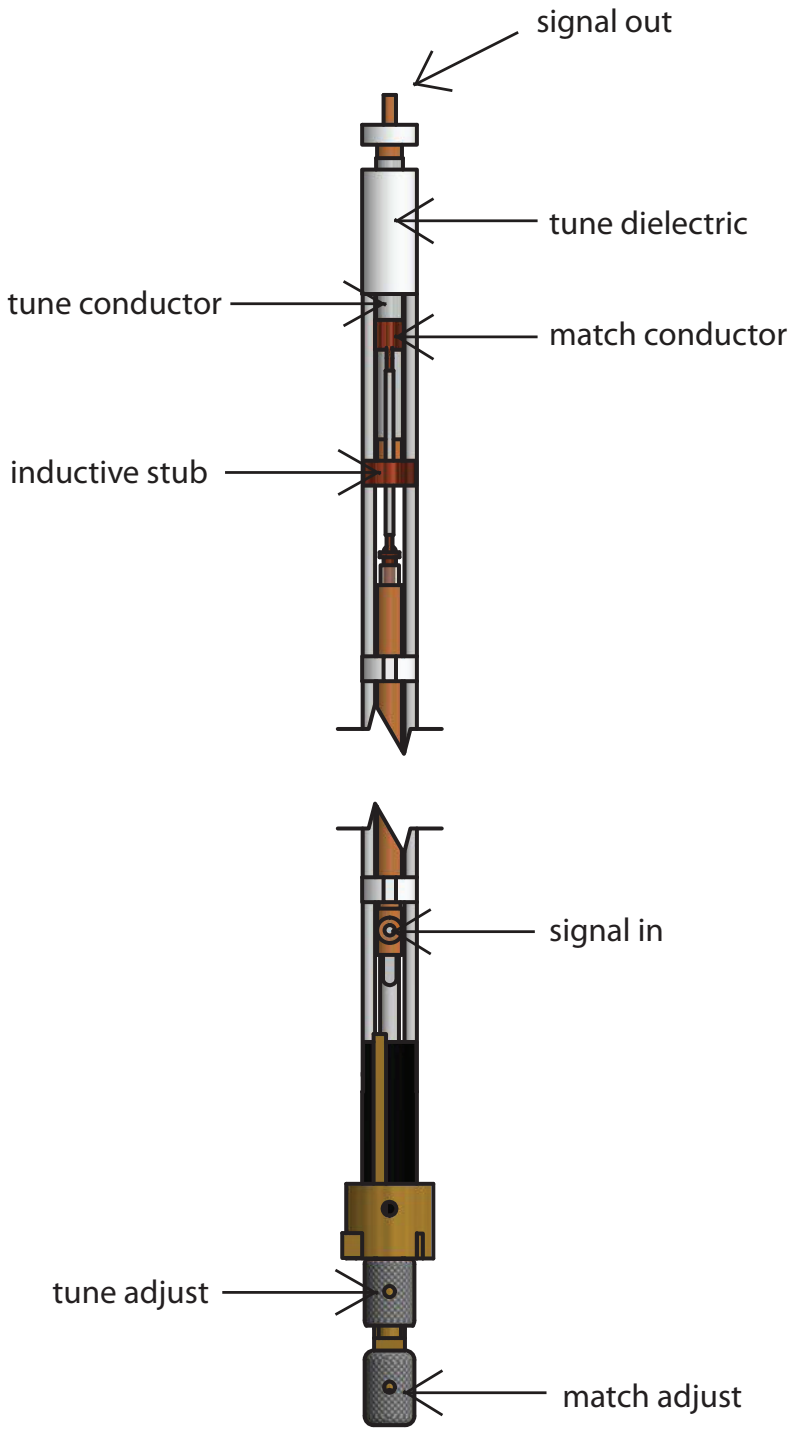

Figure 2.17: Front view of the assembly of tuning, match, and structural elements of the ^{1}H channel; the middle of the schematic has been removed due to space constraints.

As shown in Fig. 2.17, the presence of the inductive stub requires a different mechanism for the match capacitance. Instead of the uppper match conductor feeding into the tune conductor, as in the heteronuclear channels, the upper match conductor is a small cylinder that fits over the tune conductor. The small wires that connect the lower match conductor to the upper match conductor pass through small holes in the inductive stub, which is soldered to the tune conductor. The arrangement of guide rods, rf feed, and tune dielectric is the same as in the heteronuclear channels.

Chapter 3

Benchtop Probe Characterization

Constructing an NMR probe is an iterative process of machining components, assembling them sufficiently to conduct benchtop measurements, staring at bewildering results, and constructing new components with altered dimensions until the world makes sense again. The length of this process increases exponentially with each channel added to the circuit. Calculations can be used to predict the required dimensions, but the complexity of the interactions between the channels within the probe circuit, and stray capacitances and reactances from other probe components, ensure that a number of iterations will be required.

3.1 Coil Inductance

Given that the probe is built around the coils, the inductance of the coils must be measured to have an idea of what value of capacitances the channels will require. Coil inductance can be measured by building little resonant circuits composed only of the coil and chip capacitors.

Figure 3.1: Small LC circuit in the "magic box" used to measure resonant frequency.

The resonant circuit is then placed in a shielded box with a wire loop on either side as shown in Fig. 3.1. These loops are used as broadcast and pickup antennae with a spectrum analyzer.

This allows the resonant frequency of the circuit to be measured. Swapping out the chip capacitor allows a plot of $\frac{1}{f^2}$ as a function of C to be generated, yielding a line whose slope is the inductance of the coil.

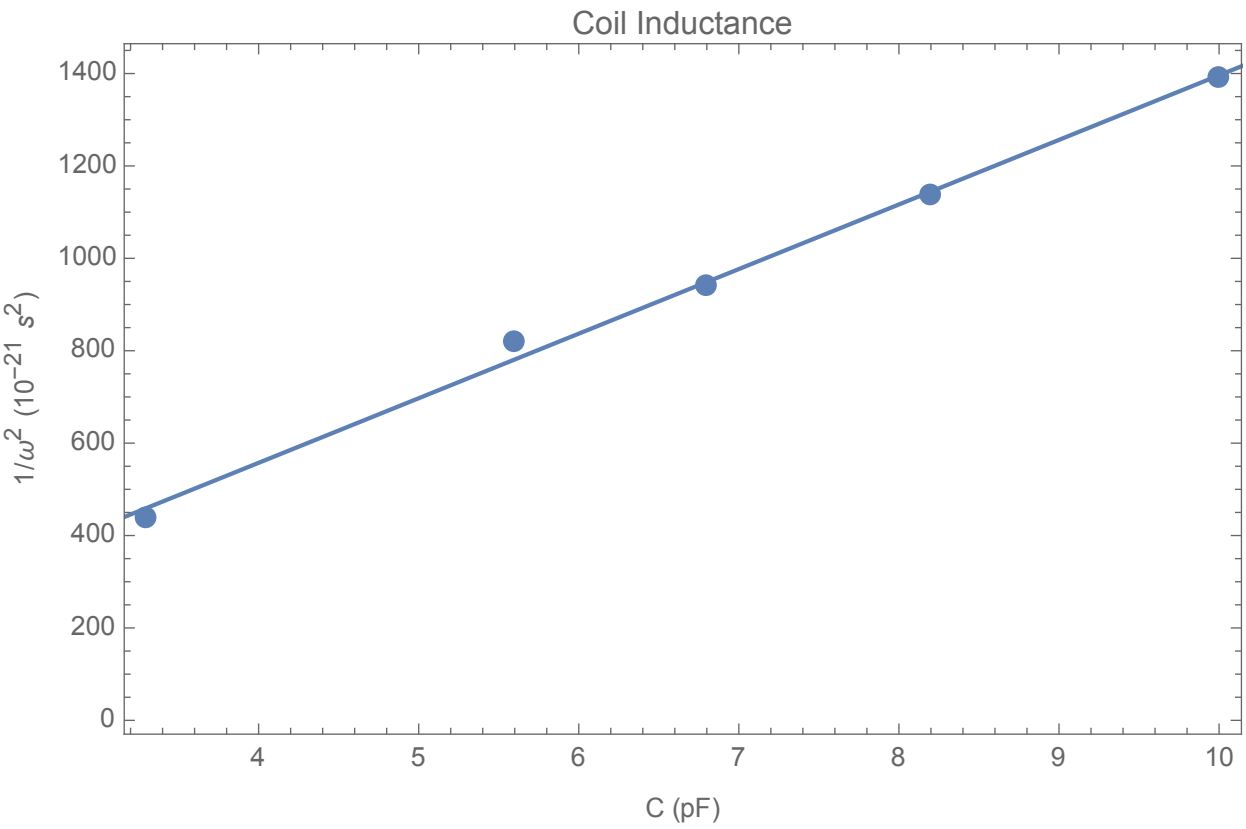

Figure 3.2: Plot of square of inverse frequency against capacitance used to calculate the inductance of the signal coil.

3.2 Tuning

At the coarsest level the resonant frequency of each channel is determined by the physical dimensions of the components.

$$C = 2\pi\epsilon_r \frac{1}{ln\frac{b}{a}} l \tag{3.1}$$

The dimensions subject to modification are the diameter of the outer layer b, the inner diameter a, and the length l. Additionally, the vertical motion of a dielectric cylinder between two conducting layers can change the capacitance by changing the dielectric constant ϵ_r.

The diameter of the outer grounded tube that contains the channel is standardized by the sincere desire to only build the probe frame once. The lengths and diameters of the transmission line segments contained within the tube, however, can be altered as necessary to allow the circuit to tune and match to the desired frequency. This is one of the primary motivations to machine the parts directly–it allows new components to made as adjustments are necessary. The first stages of the tuning process entail a period of interativelly swapping parts to reach the desired frequencies on each channel, with each change potentially affecting the other channels. Having a "library" of components of different dimensions stockpiled eases the process. Helping machine components for this library is therefore a traditional introduction to the probebuilding section of lab.

The fine tune and match adjustments needed to adjust the probe for experimental conditions are accomplished through the vertical motion of several of the transmission line segments. Knobs at the base of each channel attach to threaded actuators. These actuators feed into the guide rods to which the tune cylinder and match conductor are attached, allowing their position to be adjusted. The length of the associated guide rods must also be carefully chosen to allow a useful tuning range. Again, having a stockpile of rods of different lengths available is essential.

Reflectances were measured on an Agilent Technologies E5061A Network Analyzer to verify the tuning of each channel, and especially that all four channels could be tuned simultaneously. A frequency sweep is broadcast to the channel and the intensity of the response measured in a decibel scale.

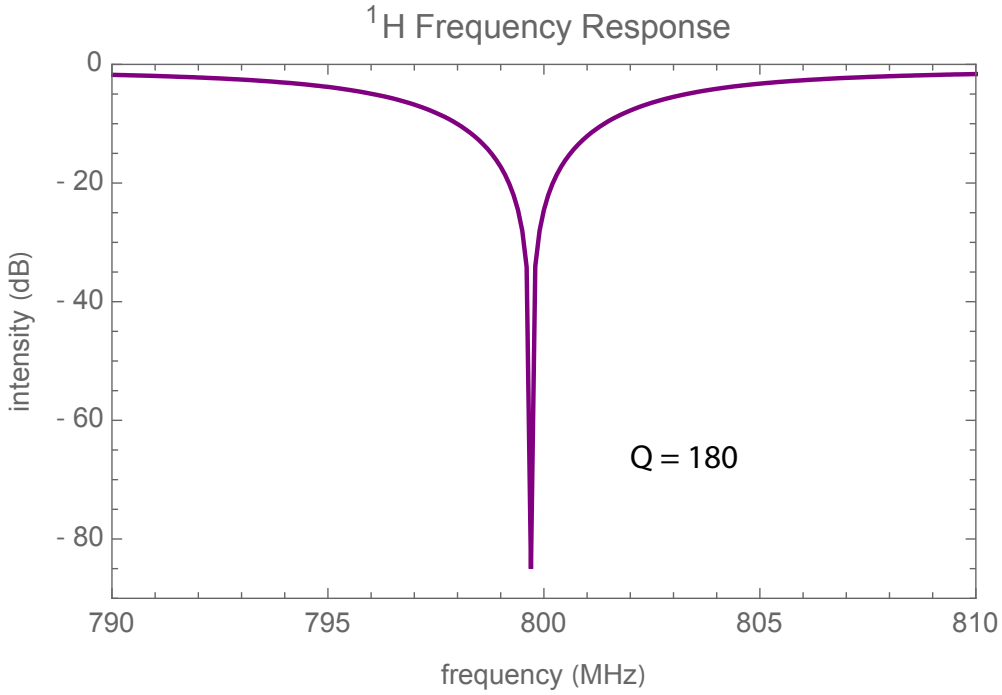
^{1}H Frequency Response
0
- 20
- 40
- 60
- 80
intensity (dB)
Q = 180
790
795
800
805
810
frequency (MHz)

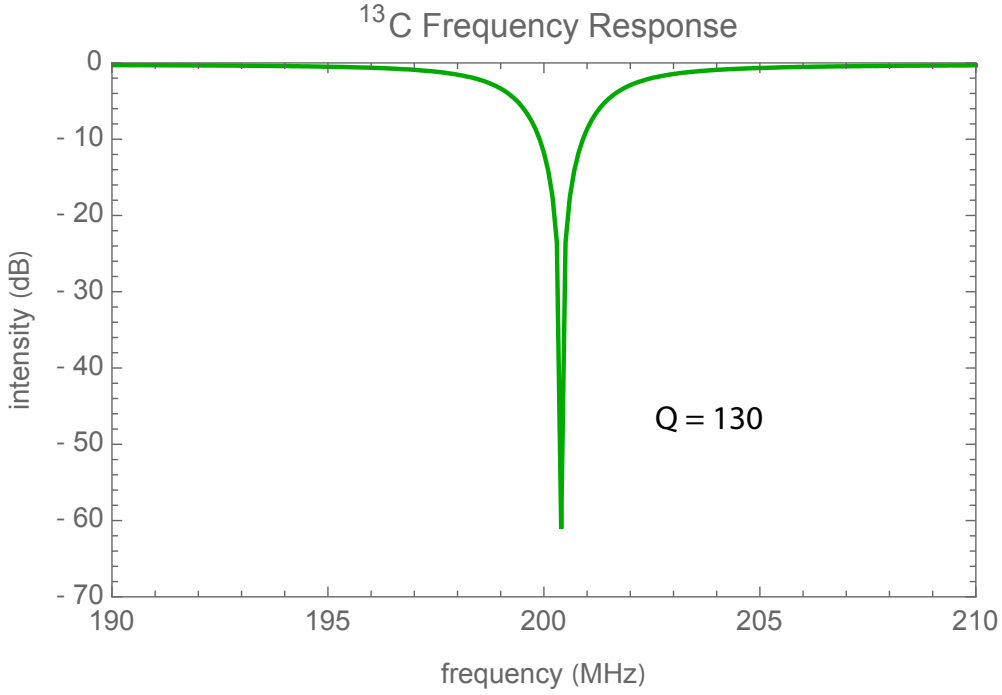
^{13}C Frequency Response
0
- 10
- 20
- 30
- 40
- 50
- 60
- 70
intensity (dB)
Q = 130
190
195
200
205
210
frequency (MHz)

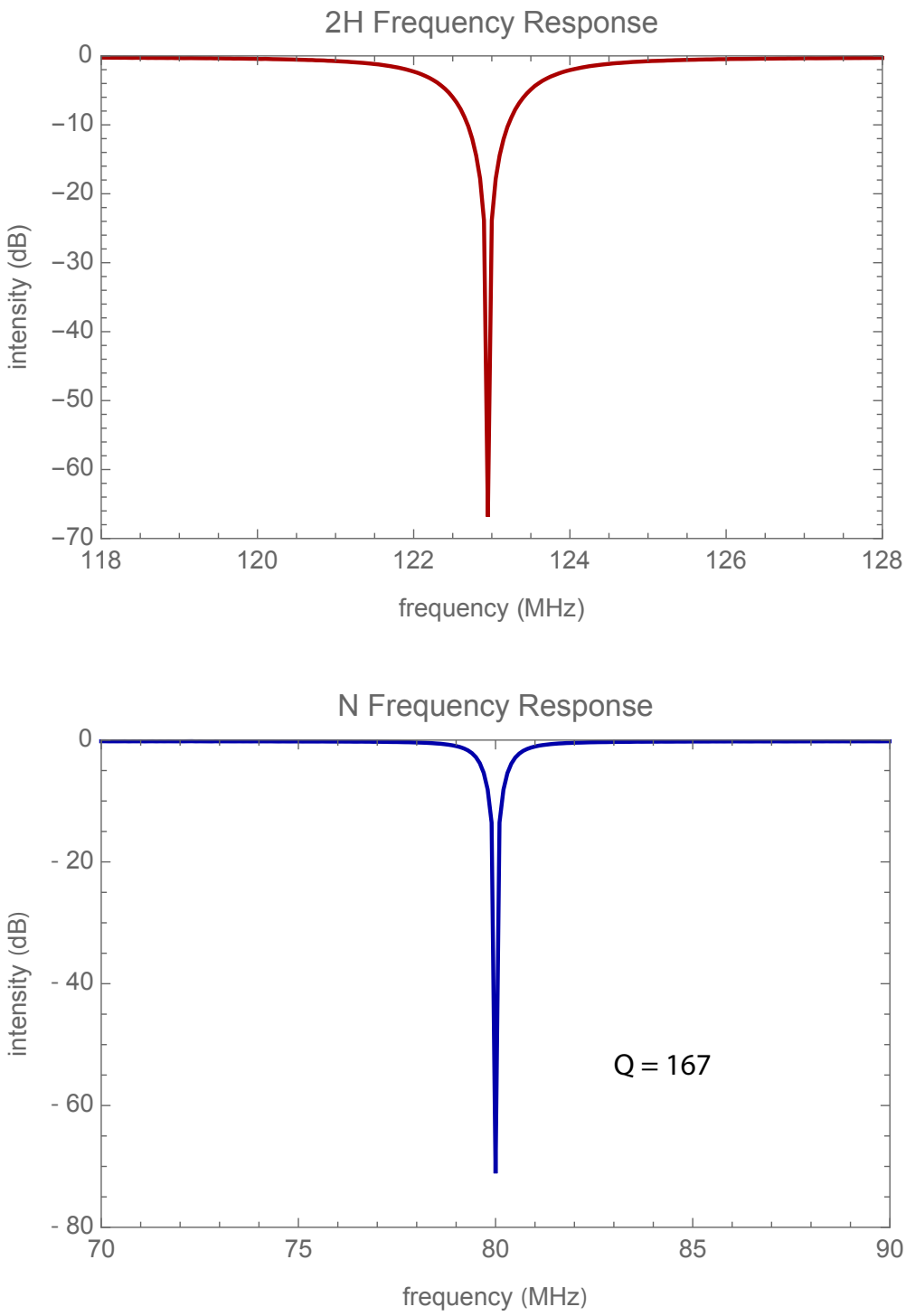

Figure 3.3: The reflectance of each channel measured on an Agilent Technologies E5061A Network Analyzer.

The tune knob is used to adjust the resonance frequency, causing a horizontal shift in the reflectance peak. The match is used to maximize the intensity of the response; the corresponding narrowness of the peak ensures that as much of the signal as possible is on resonance with the nuclei. This can be measured quantitatively by calculating the Q-value of each channel, defined as:

$$Q = \frac{2\omega_0}{\Delta\omega} \tag{3.2}$$

which serves as a measure of the efficiency of each channel.

It is important not only that the copper and dielectric components serving as capacitors and dielectrics have the correct dimensions but also that their guide rods have the correct lengths to allow a tune and match range around the desired frequency. Inserting the probe into the bore of the magnet changes the resonant frequencies of the channels slightly, and different samples of course have different chemical shifts, so a range is necessary. If the range of adjustment is too far to one side or the other, it may not be possible to tune the channel in the magnet.

3.3 Isolation

The network analyzer can also be used to measure the isolation between the channels. For this test, the frequency sweep is broadcast on one channel and the response intensity measured on another.

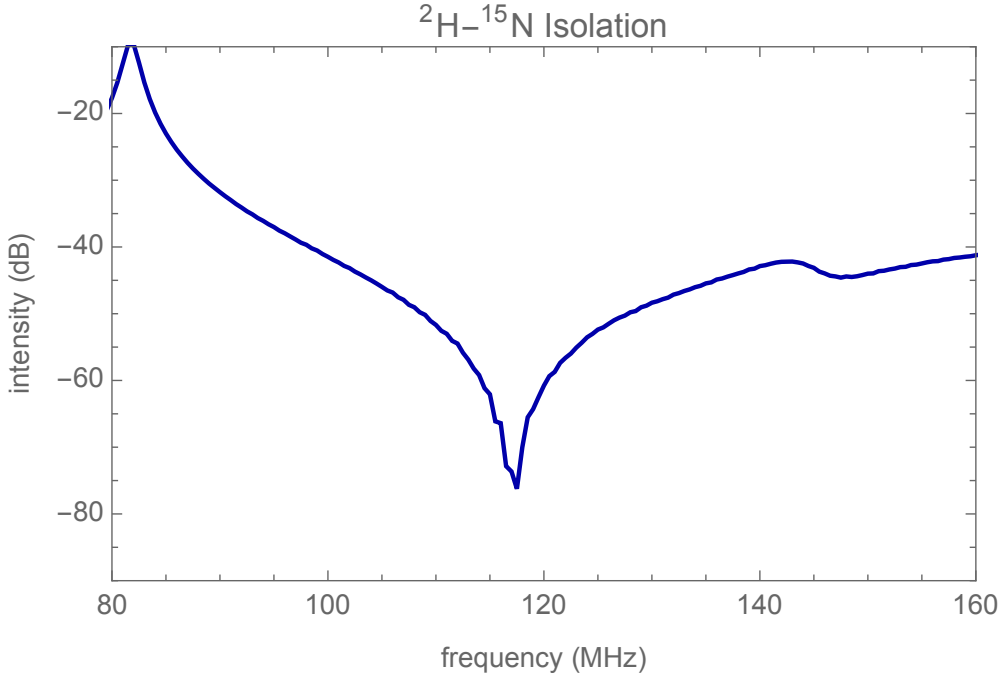

(a) Isolation between ^{2}H and ^{15}N channels.

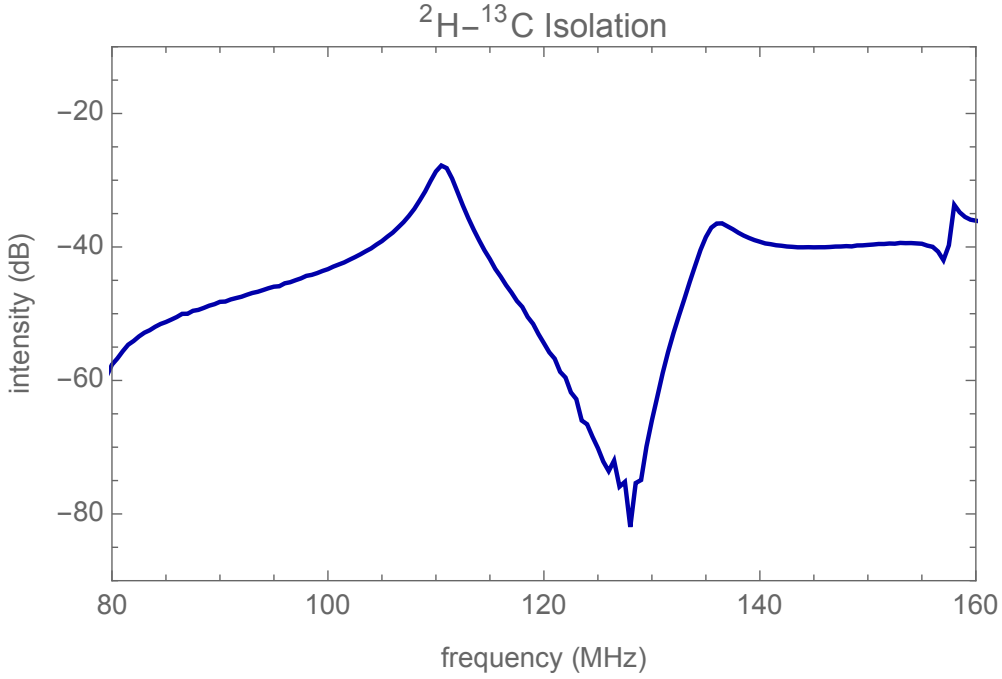

(b) Isolation between ^{2}H and ^{13}C channels.

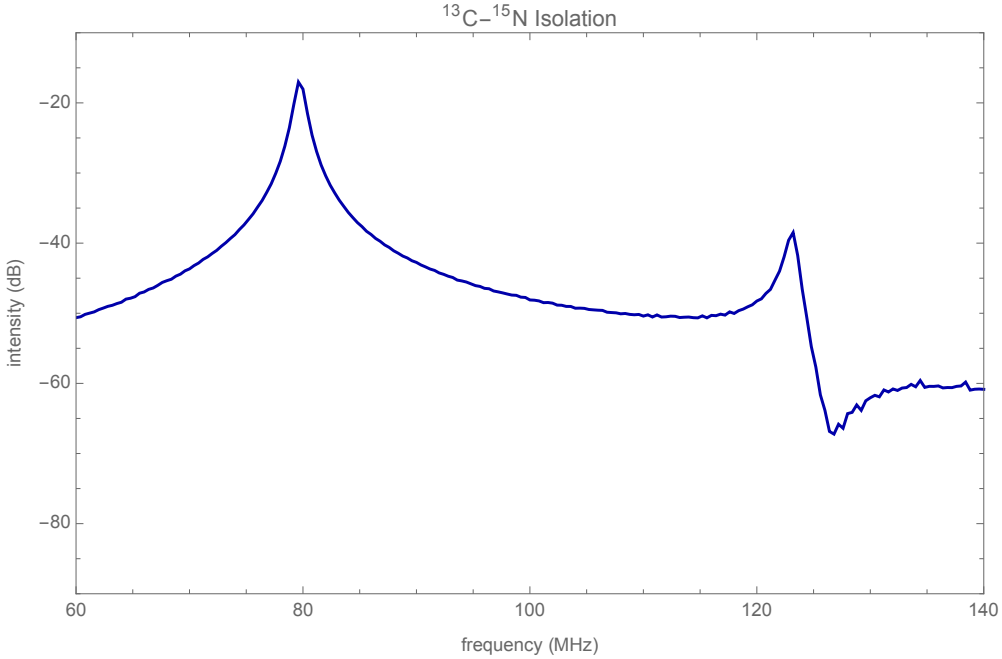

(c) Isolation between ^{13}C and ^{15}N channels.

Figure 3.4: Isolation between the probe channels.

The goal is to minimize the response at the frequency of the broadcast channel on that of the receiving channel. Ideally the actual minimum can be moved to that frequency, but the

circuit will function if the frequency is on the negative slope of the response.

3.4 Coil Homogeneities

Once the probe is tuning, the homogeneity of the coils can be measured. This determines the region in which the sample must be restricted to prevent inhomogeneities in the B_1 field from affecting the data. It is also important that the homogeneous regions of the two coils have as much overlap as possible; this is the region in which cross-polarization, decoupling, and multidimensional experiments will be effective. Any sample present ouside of this region will distort the results.

In the ball-shift method, coil homogeneity is measured by moving a small copper disc through the coil and measuring the change in frequency. The disc is placed at the end of a threaded rod that is rotated through a holder attached to the front of the stator. This allows the displacement of the disc to be precisely calculated.

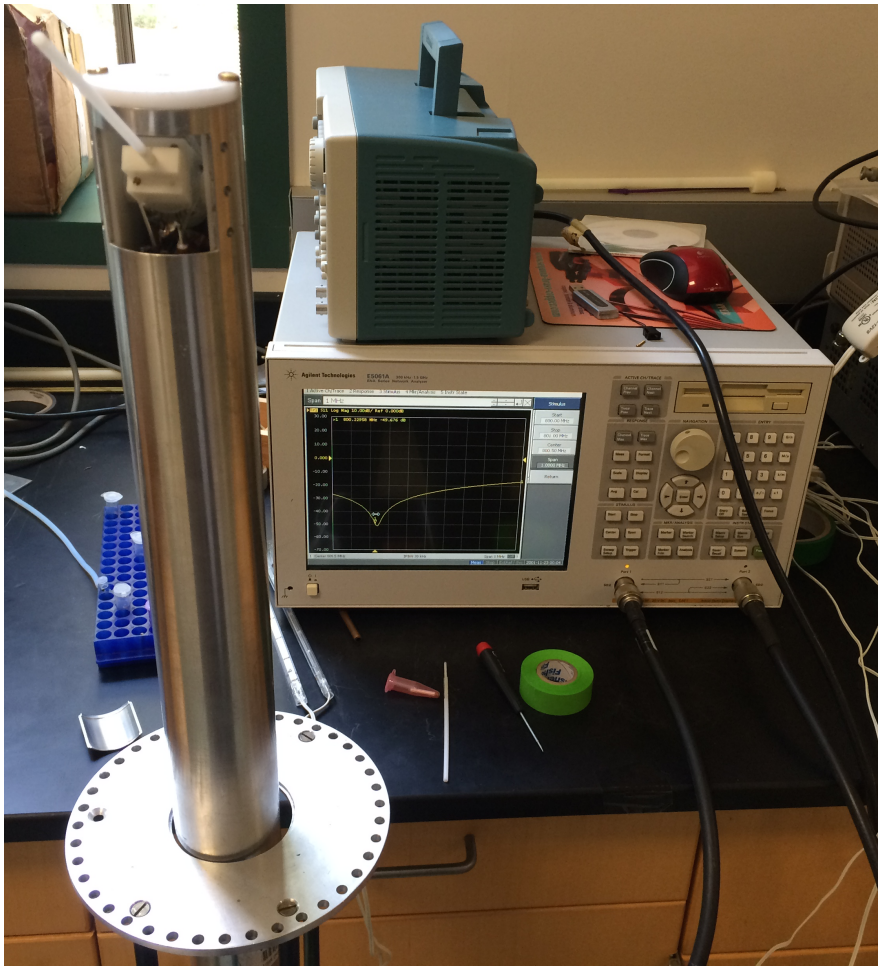

Figure 3.5: The assembly used to measure coil homogeneity.

Plotting the magnitude of the shift in frequency against the displacement of the coil generates a map of the homogeneity (hopefully) of the coil. The "plateau" region is the area to which the sample must be restricted.

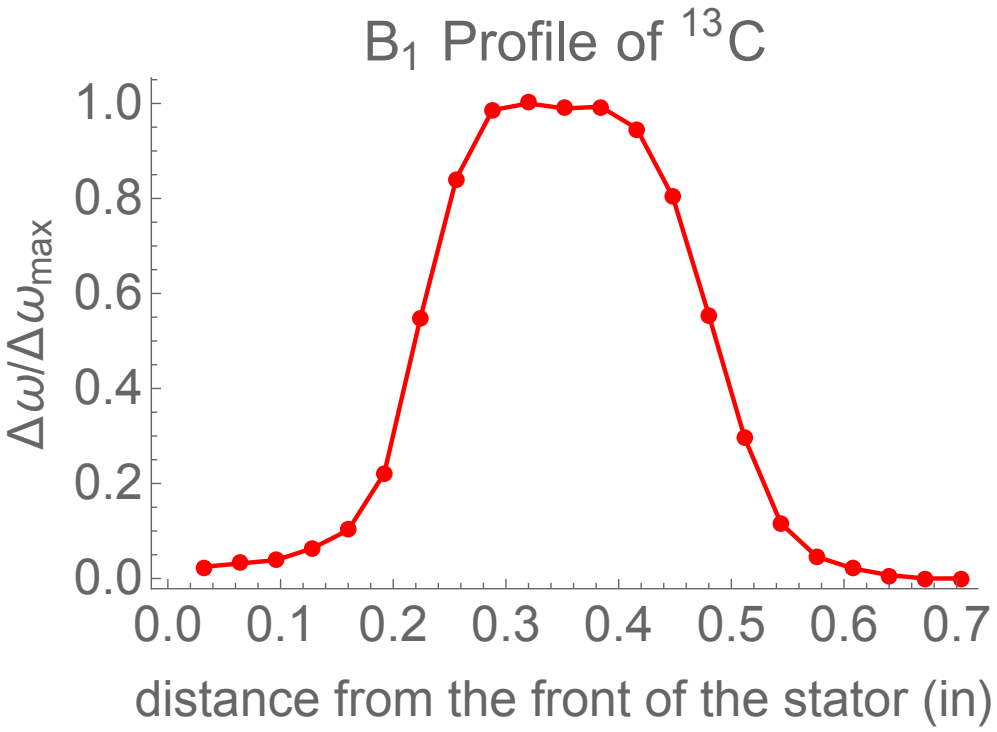

Figure 3.6: Homogeneity measurement performed on the ^{13}C channel.

This is not what the first several (hundred) measurements looked like. Complicating factors include the alignment of the coils in the stator, the alignment of the coils relative to each other, and the balancing of each circuit, as well as possibly the phases of the moon.

Obviously the physical alignment of the coils in the stator is a major determinant of their homogeneity. If the coils are tilted relative to the stator, the plateau becomes a sad little hill.

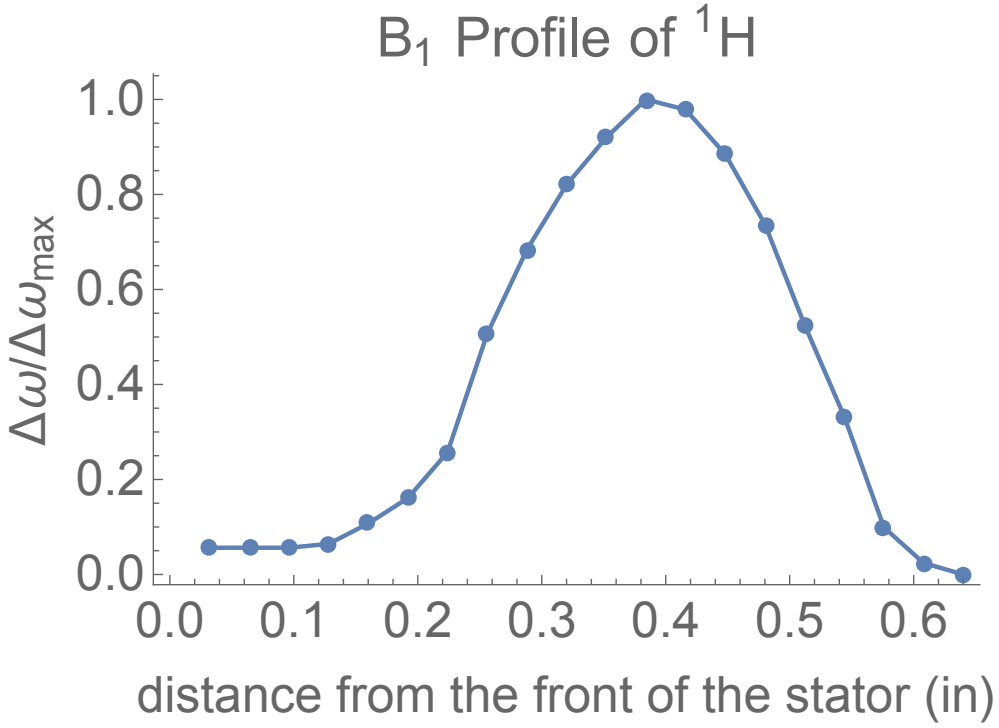

(a) (Non) homogeneity on ^{1}H channel.

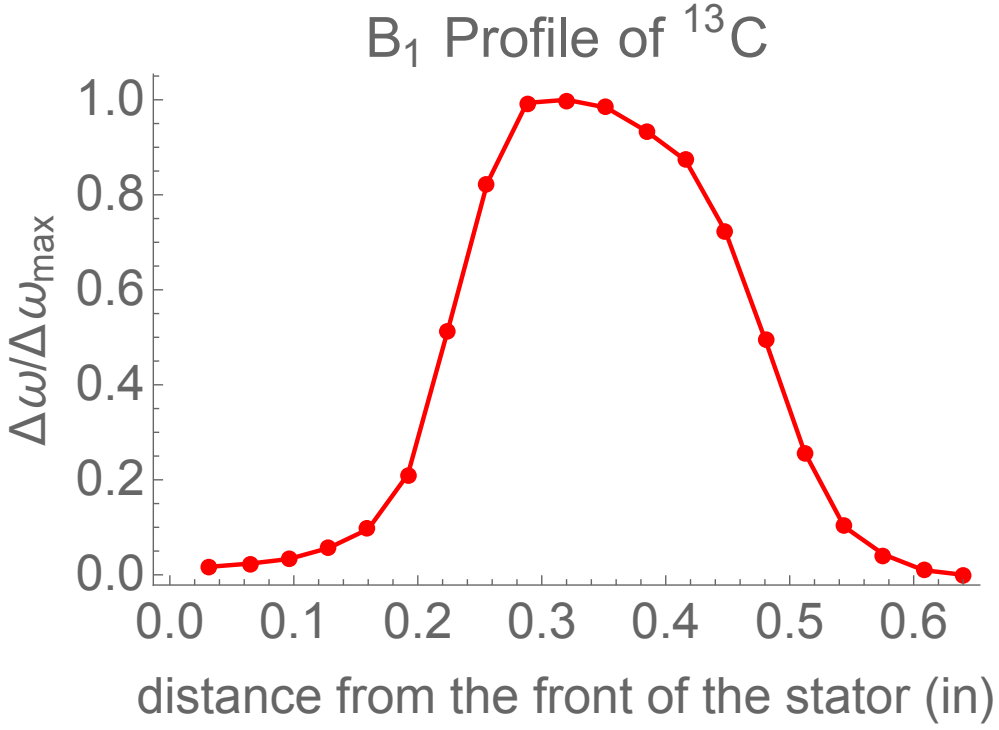

(b) (Non) homogeneity on ^{13}C channel.

Figure 3.7: Homogeneity plots when the coils are tilted relative to the stator. The effect is particularly noticeable on the ^{1}H channel since the MAG resonator has a narrower homogeneous region.

Of course, since the coils had to be placed in the stator, there is a certain degree of freedom of motion. There is a flat Teflon holder that screws into the bottom of the stator. The legs of the coils protrude through small holes drilled in the holder. This offers some stability. The alignment of the coils msut be adjusted to optimize the spinning of the rotor. This very complex and technical process is accomplished by hunching over the probe and poking at the coils with a small wooden dowel. When the alignment is correct, the rotor will slide in without any resistance–success is marked when it becomes difficult to remove the rotor because any loss in grip will see it slide back in.

If the two coils are shifted relative to each other, so that one is sitting a little forward of the other, there may be little to no overlap of their homogeneous regions.

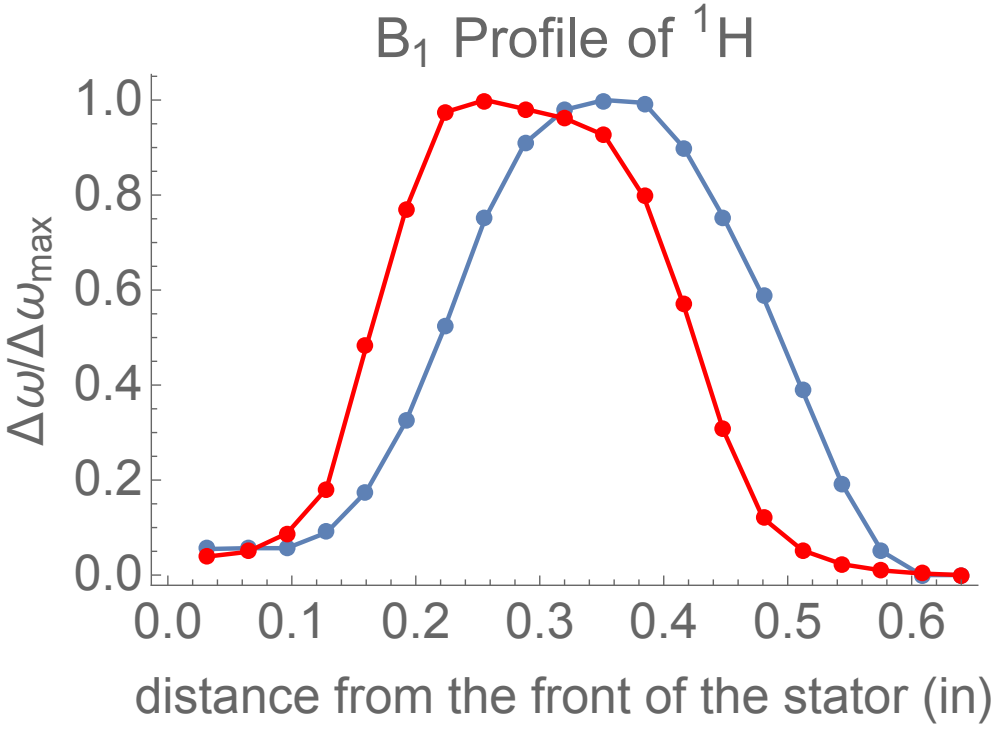

Figure 3.8: Homogeneity plot of the coils when they have a relative shift–note the lack of overlap of their homogeneous regions.

This would not be a good configuration in which to attempt cross-polarization, decoupling, or any kind of multi-dimensional NMR. It also poses the fun question of which region of the

rotor to pack the sample in.

In the ideal case the homogeneous regions of both coils are as broad as possible and completely overlap.

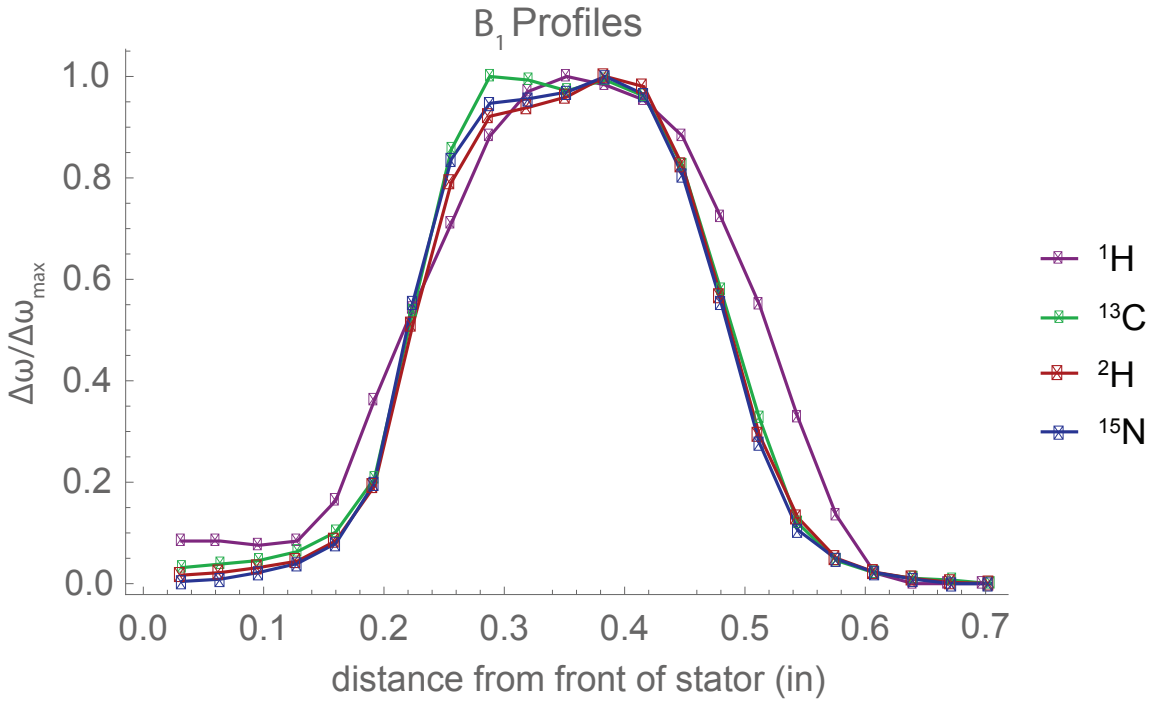

Figure 3.9: Homogeneity measurements performed on all four channels of the probe.

In this configuration it is possible to do fun things like spin the rotor and perform cross-polarization and decoupling experiments.

Chapter 4

Experimental Probe Characterization

Once at least one channel of the probe is matching and tuning on the benchtop, the moment of truth arrives: placing the probe in the magnet and attempting to detect the signal from a sample. Of course there's a bit more to it than that.

4.1 1D Spectra

Before a spectrum can be taken the probe must be tuned and matched in the magnet. On the benchtop, this is done by viewing the frequency response on a spectrum analyzer. In the magnet, this is done by minimizing the ratio of the reflected voltage to the input voltage. These voltages are measured at the directional coupler that signals are passed to and fro through between the console and the probe. The measurements are performed with a Tektronix TDS5104B oscilloscope.

The input voltage is kept low for the initial tuning and matching. Once the reflected voltage has been reduced to less than 10% of the input voltage, the voltage can be carefully raised. The reflected voltage must be carefully monitored; a sudden spikiness indicates arcing some-

where in the probe circuit, and the voltage must immediately be lowered to prevent damage to the probe or sample. Sometimes arcing is the result of physical imperfections that can be corrected, making higher power levels possible, but eventually a limit is hit. Higher power results in a shorter 90-time, allowing experiments to be completed more quickly. Given that multidimensional experiments can run for several days, anything that saves time is important!

Once the probe is tuning and the power level is high enough for experiments to be conducted in a reasonable amount of time, the "sweet spot" can be determined. This is the vertical position of the probe in the magnet in which the field is the most homogeneous. The position of the probe in its frame is controlled by set screws, allowing it to be adjusted even when the frame is screwed to the base of the magnet. To find the sweet spot, the probe is carefully raised into the magnet with incremental changes in elevation. At each position, a spectra is taken with the z-shims at zero and at relatively large positive and negative values. Changing the shim value causes a positive or negative change in frequency. By graphing these shifts it is possible to find an intersection where there is no shift; this is the position at which the field is homogeneous.

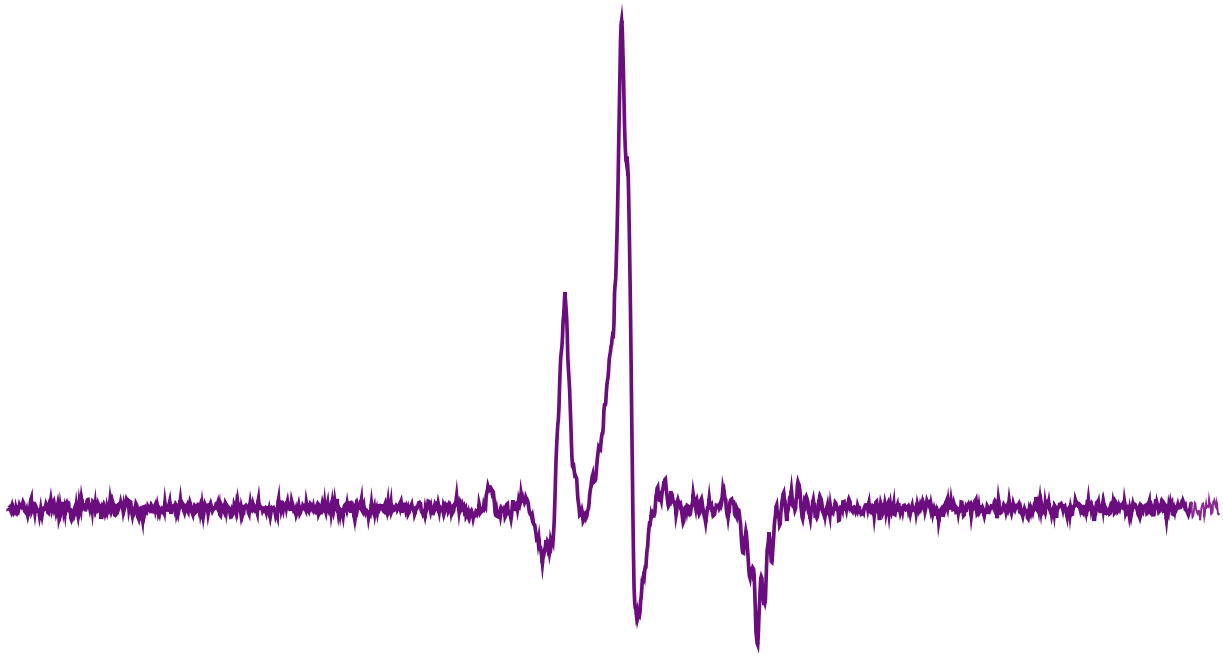

(a) Probe located below the sweet spot.

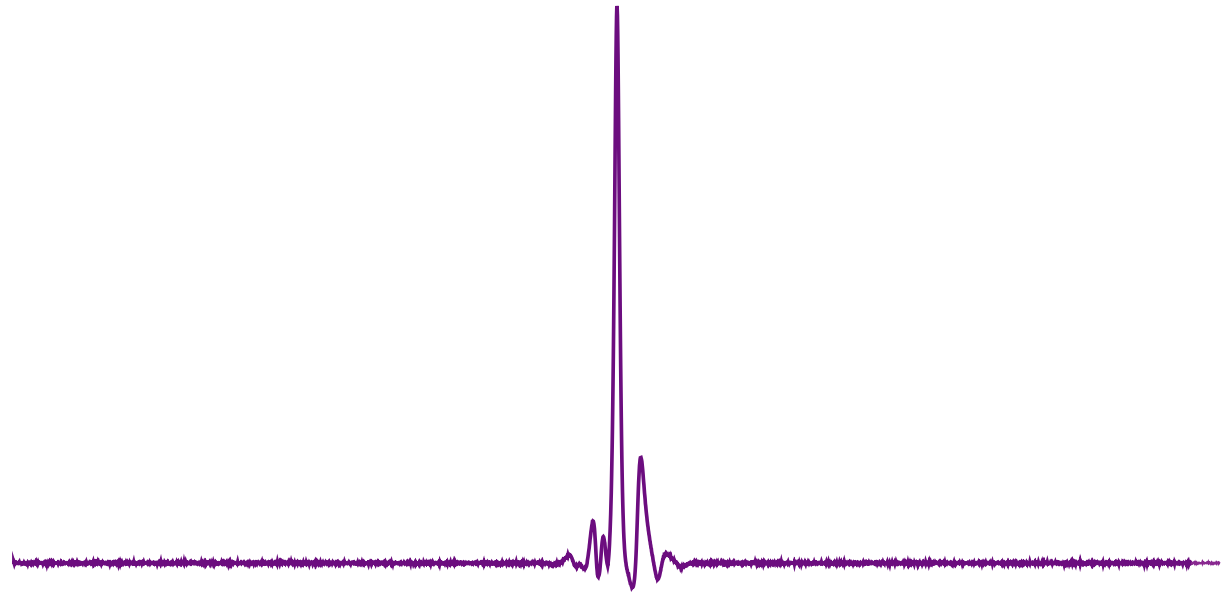

(b) Probe raised to the sweet spot.

Figure 4.1: Simple one-pulse experiment on the ^{1}H channel with an adamantane sample spinning at 6 kHz.

As can be seen in these spectra, setting the sweet spot makes a significant difference in signal homogeneity and strength. The spectrum in Fig.4.1 exhibits a significantly better signal-to-

noise ratio; plotting it to fit on the screen rescaled it such that the noise in the baseline is barely visible, compared to Fig.4.1a.

The stator must be set to the exact magic angle. This is done by adjusting the angle of the stator while viewing the spectrum of KBr, which has many spinning sidebands–when viewed at the magic angle. Although this probe dose not have a Br channel, the nutation frequency of Br is very close to that of ^{13}C, making it possible to retune the channel for the experiment. These sidebands can be seen in both the raw data of the FID and the processed spectrum.

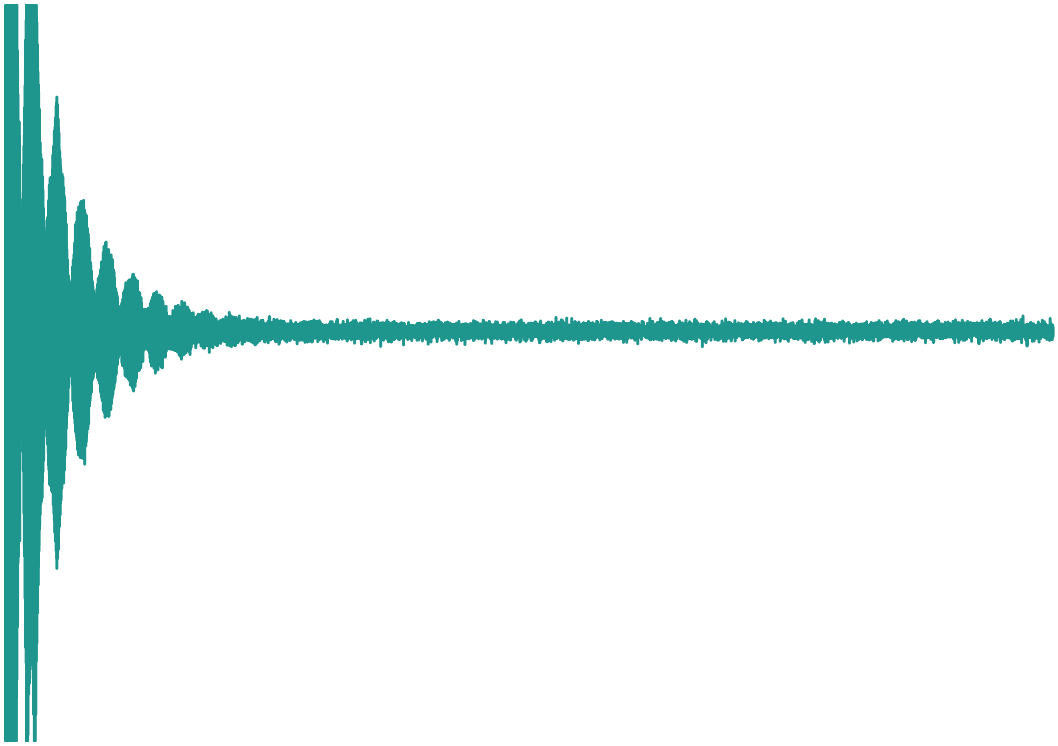

(a) FID signal.

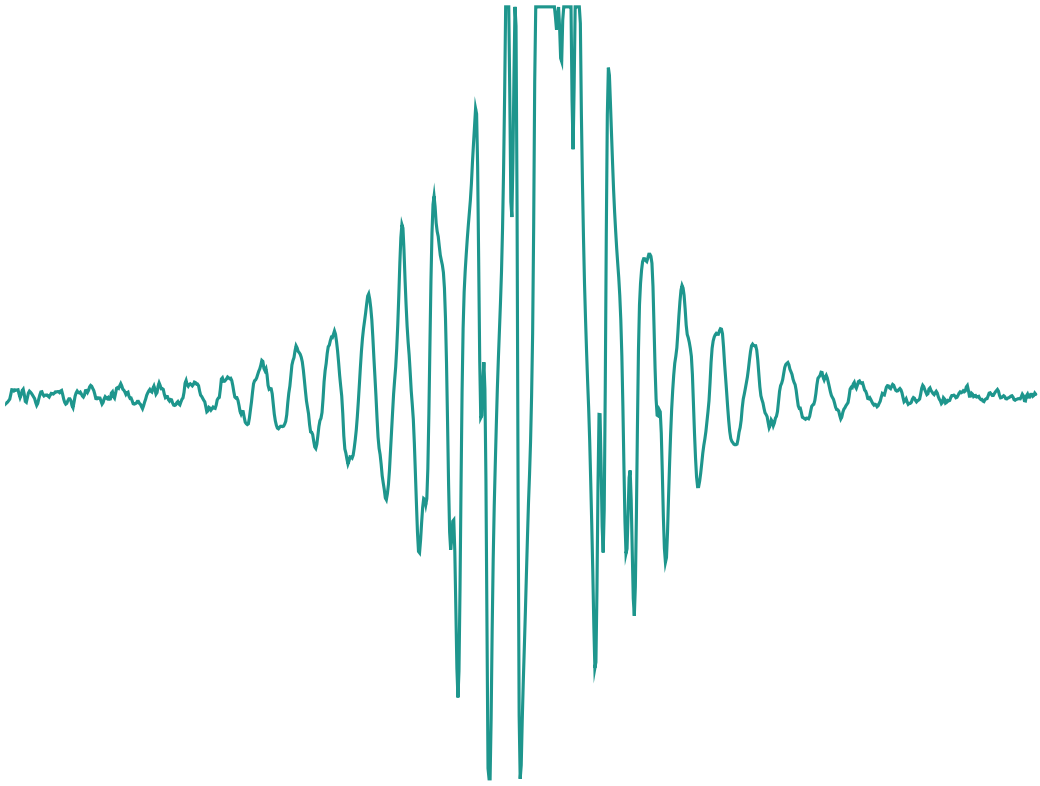

(b) Zoomed-in view of the spectrum.

Figure 4.2: Simple one-pulse experiment on the ^{13}C channel tuned to Br with a KBr sample spinning at 2 kHz.

The closer the sample is to the magic angle, the more sidebands are visible. A change in angle of even fractions of a degree has a dramatic impact on the spectrum.

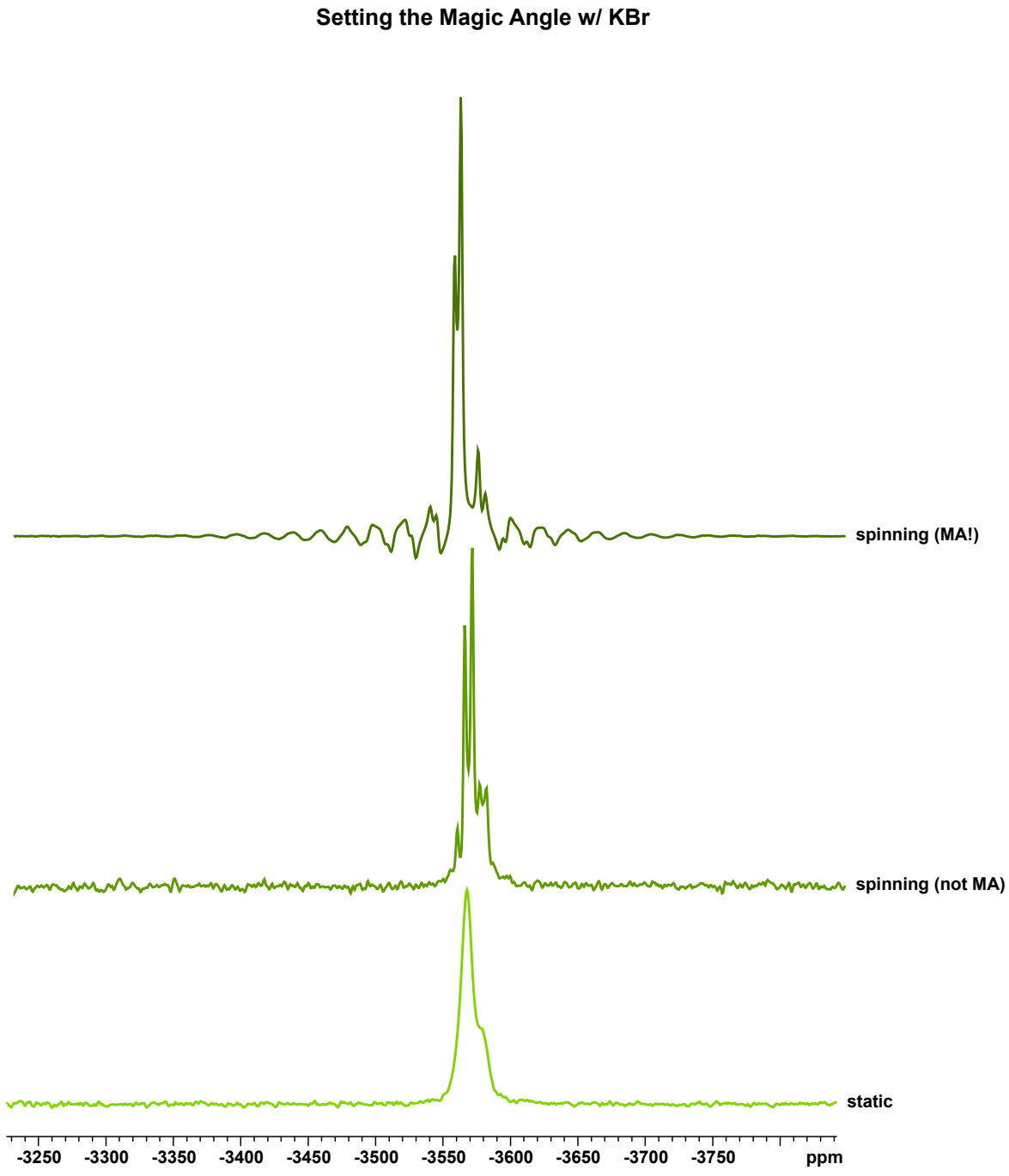

Figure 4.3: The 1-dimensional spectrum of KBr as the magic angle is set.

This readily visible effect is why KBr is used to set the magic angle. Note that there is a significant increase in signal-to-noise as well as the dramatic increase in sidebands.

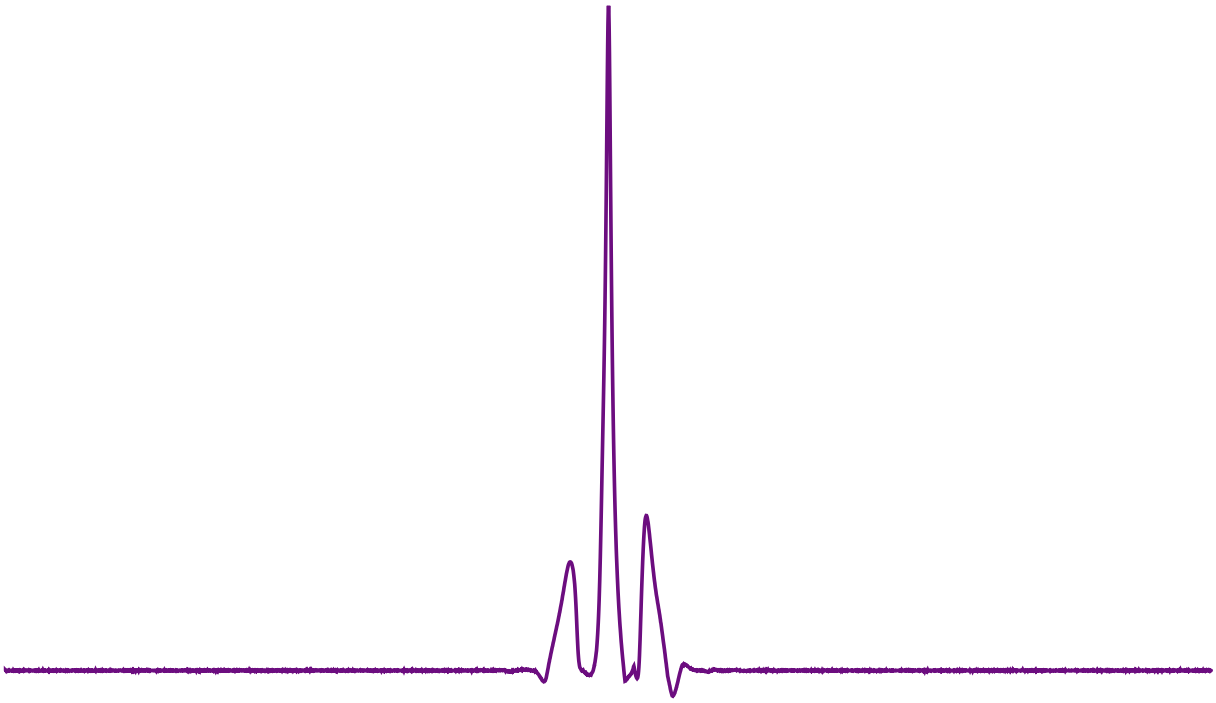

Figure 4.4: One-pulse spectrum taken on the ^{1}H channel with an adamantane sample spinning at 5.2 kHz.

Adjusting this parameter leads to another significant improvement in signal-to-noise and symmetry.

In the final step of setup, the shim coils around the probe are adjusted to maximize the homogeneity of B_0. Although there are automated programs to shim with liquid probes, for solids NMR the process is performed manually. The parameters are adjusted to maximize the intensity and symmetry of the signal peaks. As with tuning, this is an iterative process; as later parameters are changed the earlier ones must be refined.

Deuterium NMR presents an additional challenge. The quadrupolar moment of the nucleus results in a characteristic splitting of the NMR peak.

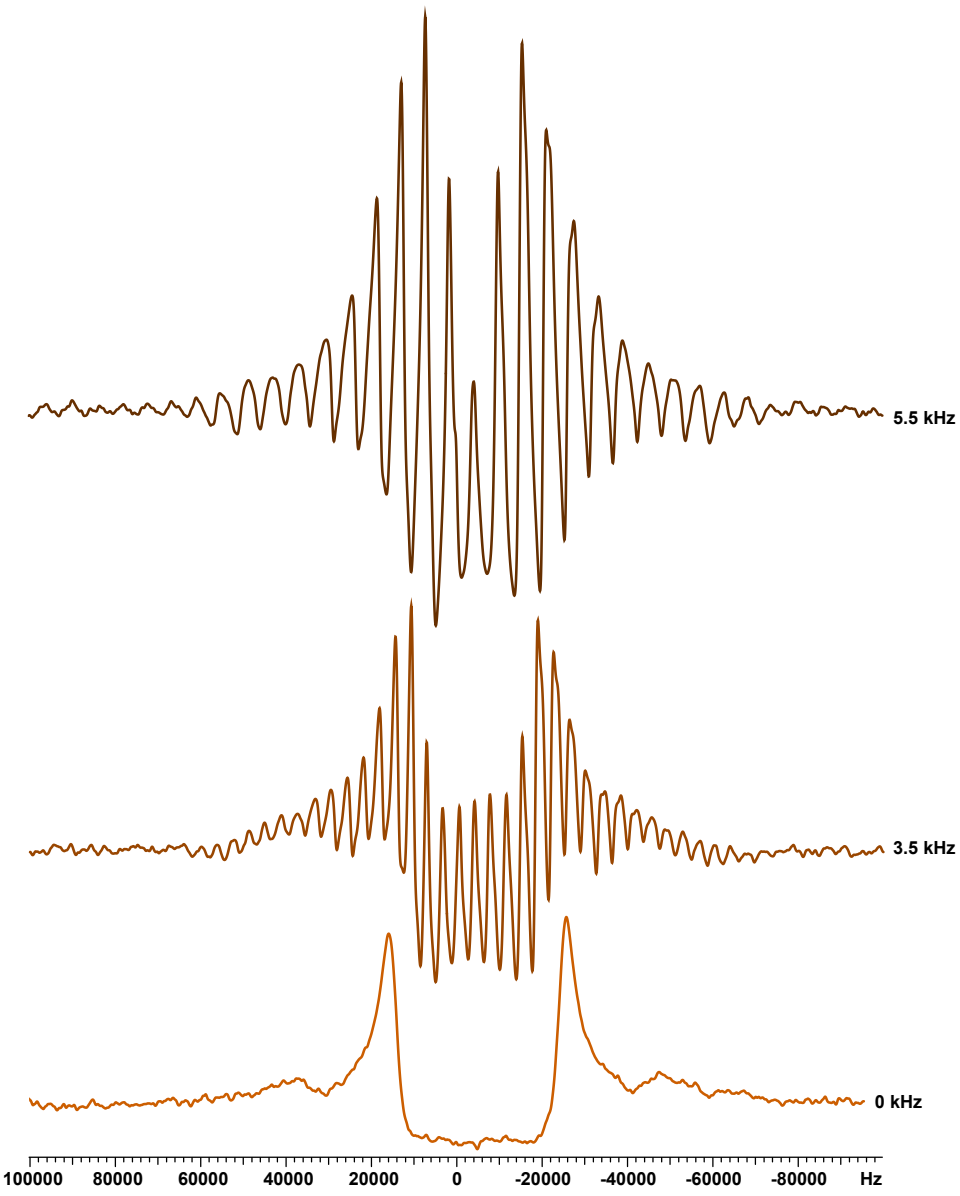

(a) Spinning series with a one-pulse experiment.

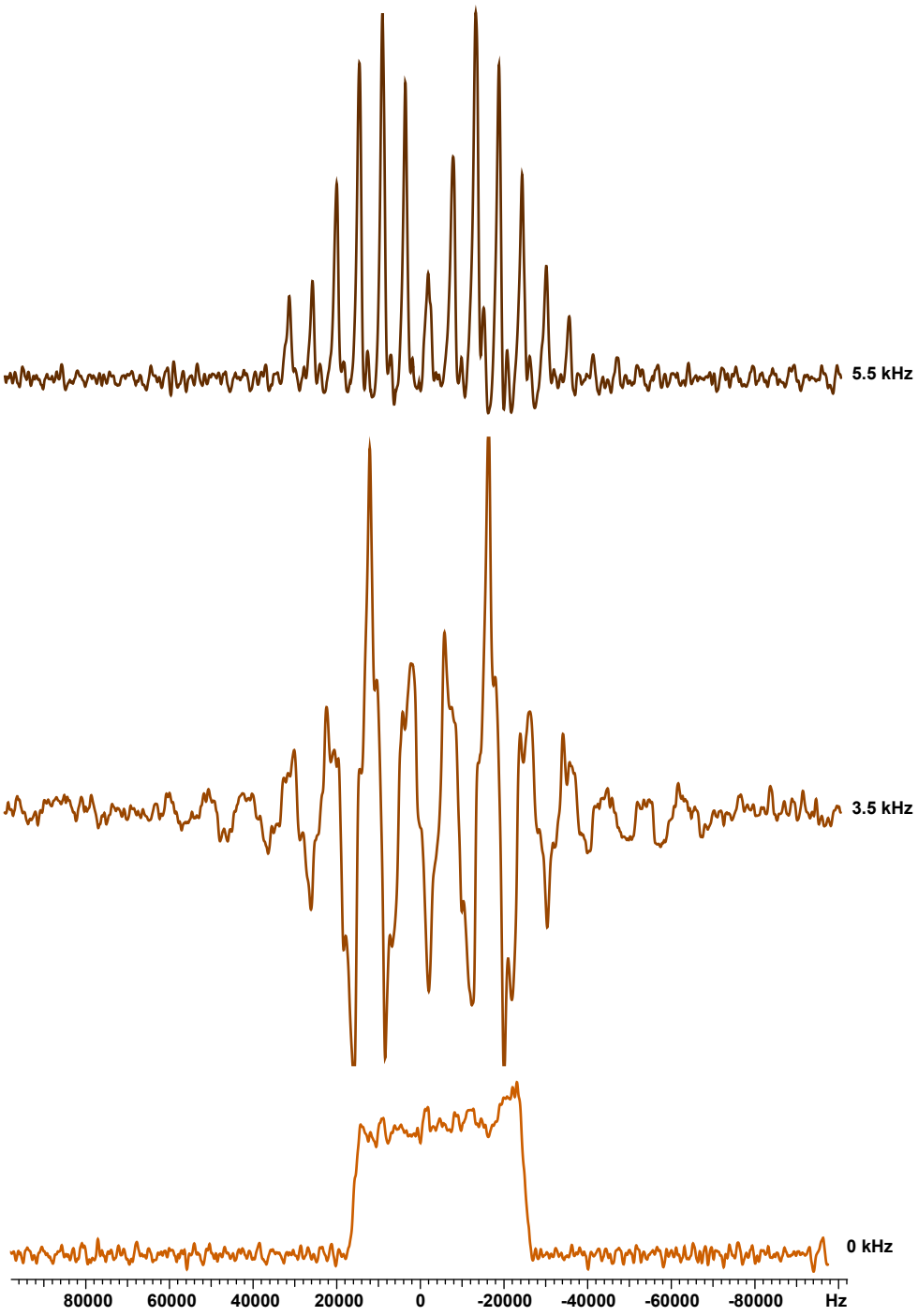

(b) Spinning series with a solid-state echo pulse sequence.

Figure 4.5: Comparison of a one-pulse and a solid-state echo sequence with ^{2}H detected on an alanine sample.

A solid-state echo sequence can be used to refocus the broadening that results from the quadrupolar moment. The narrower spectral width results in a sharper signal and easier detection.

4.2 Nutation Arrays

Once signal peaks have been detected and their appearance refined, the efficiency and homogeneity of each channel can be determined. For this, nutation arrays are taken. The most simple NMR experiment is performed–the precesssion of the spins is measured after a single rf pulse. To build the array, the length of the pulse is incremented. This tilts the induced magnetic moment of the nuclei of the sample from the z-axis, through the xy-plane, and round and round again.

Since it is the component of the spin in the xy-plane that is measured, when the spectra are lined up, the peaks follow a sinusoidal envelope.

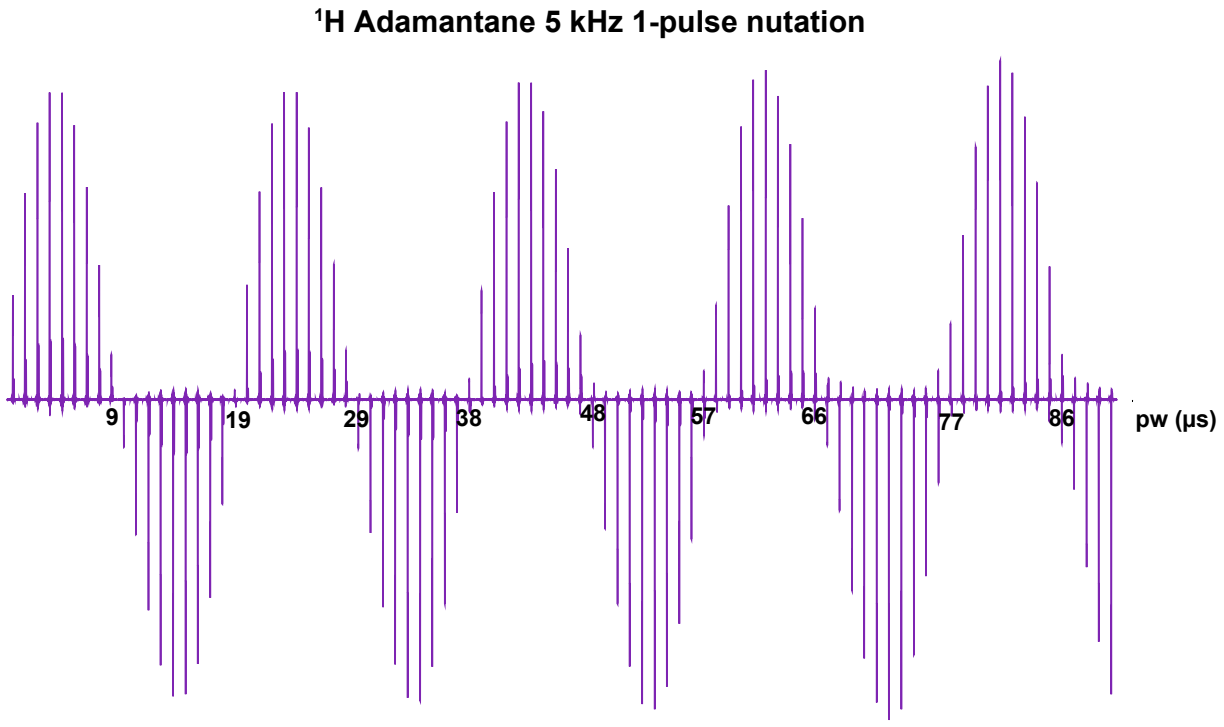

(a) ^{1}H nutation 810/90 = 0.992

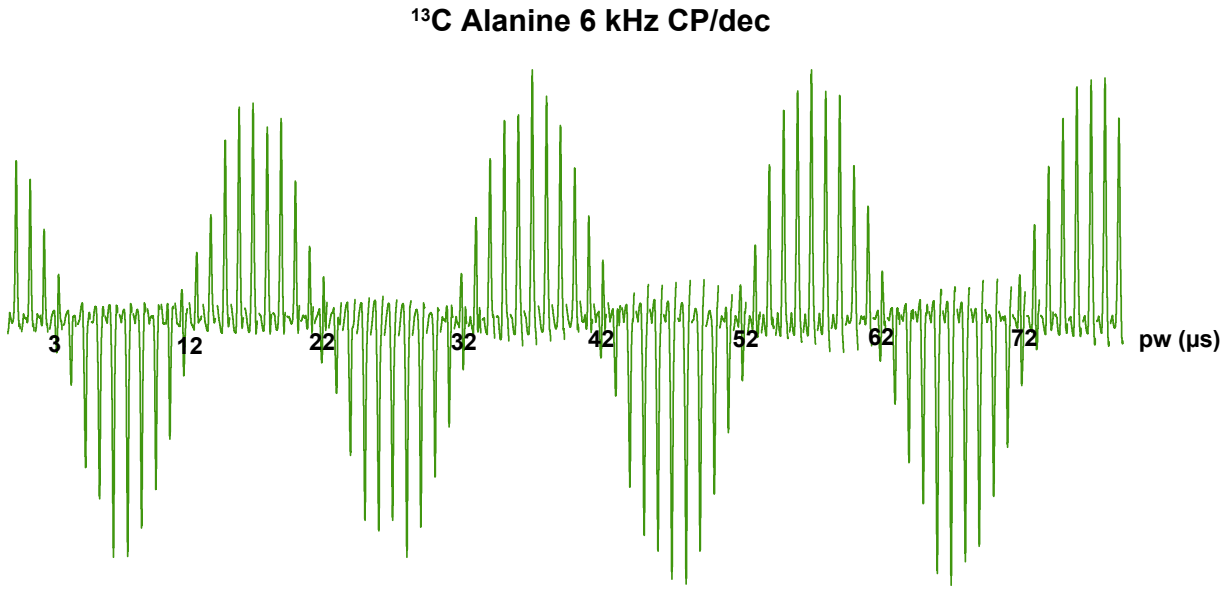

(b) ^{13}C nutation 810/90 = 0.923

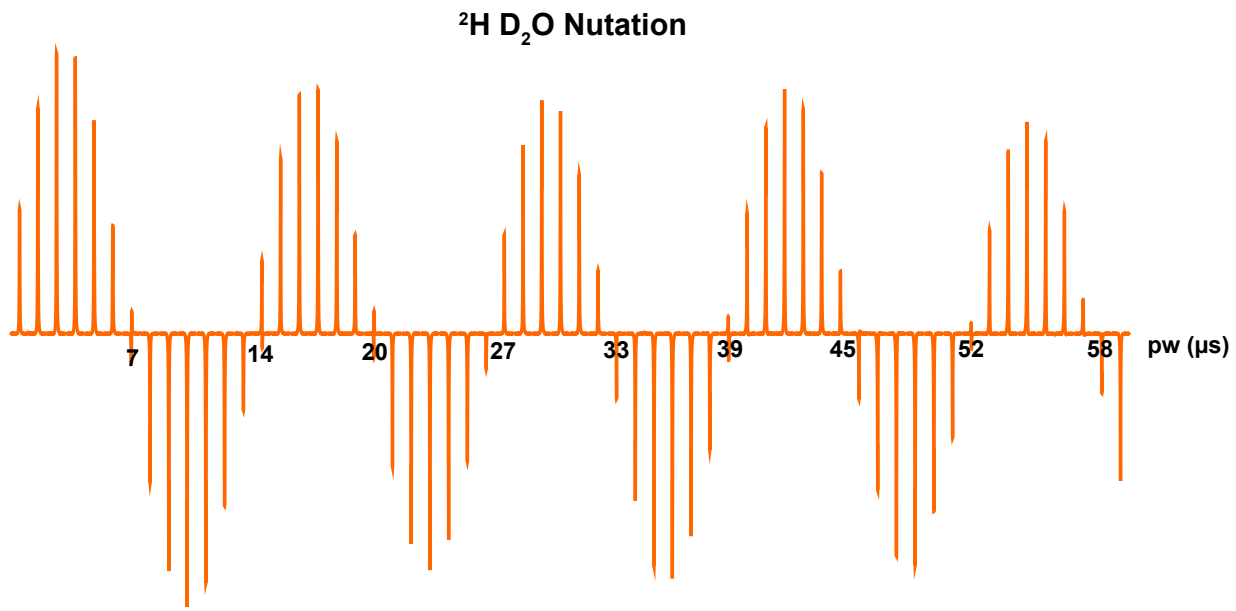

(c) ^{2}H nutation 810/90 = 0.755

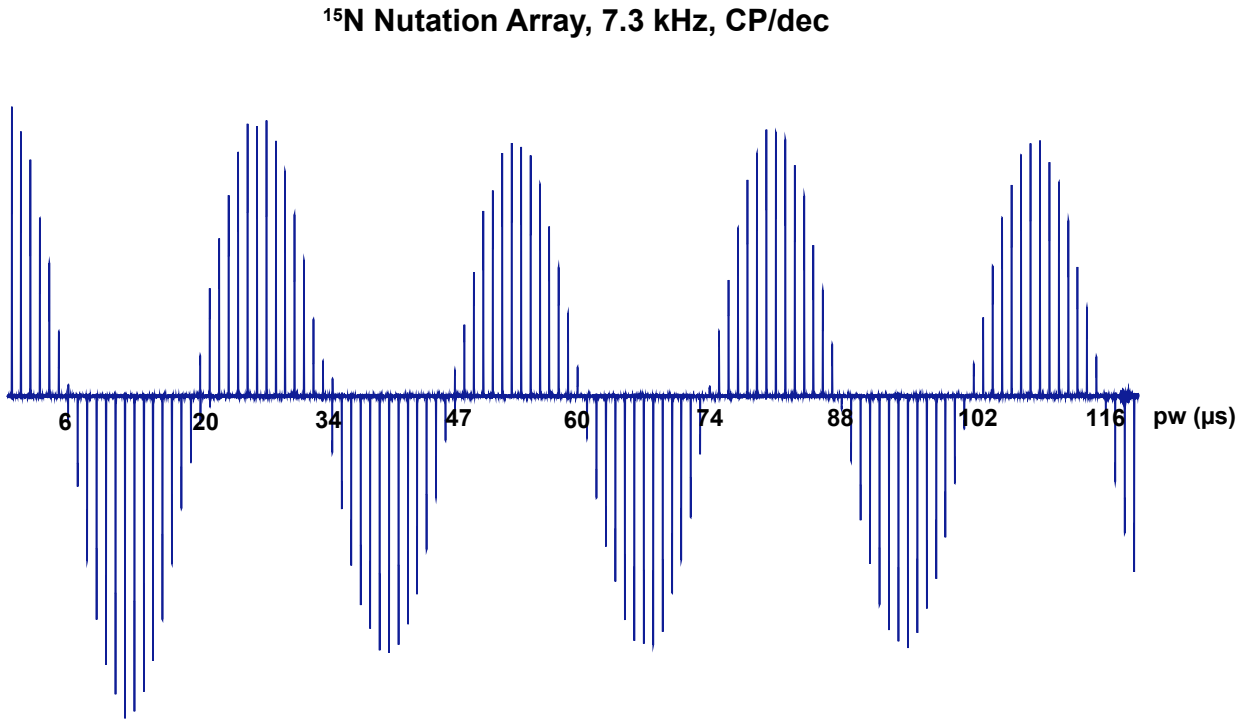

(d) ^{15}N nutation 810/90 = 0.883

Figure 4.6: Nutation arrays run on each channel.

An efficient probe shows a high frequency of this envelope, since most of the power is being

transferred to the spins. If the coil homogeneity is good (and the shims, and the sample packing...) the signal looks perfectly sinusoidal. If there is poor homogeneity, there is an additional exponential decay of the envelope. This is quantified by the 810/90, the ratio of the height the the fifth maximum to the first maximum.

4.3 Cross-Polarization and Decoupling

The most significant improvement in signal on the heteronuclei channels occurs from the use of a cross-polarization and decoupling sequence.

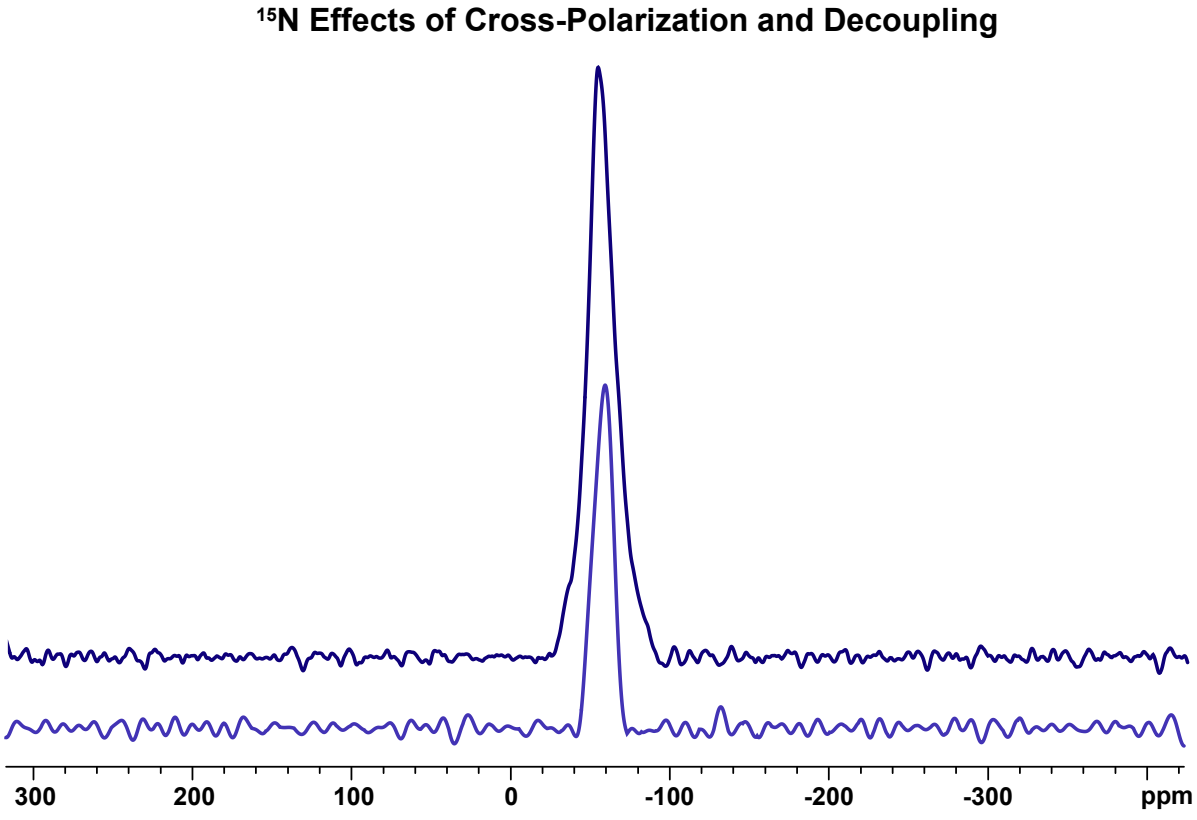

Figure 4.7: ^{1}H-^{15N} cross-polarization and decoupling compared to one-pulse experiment.

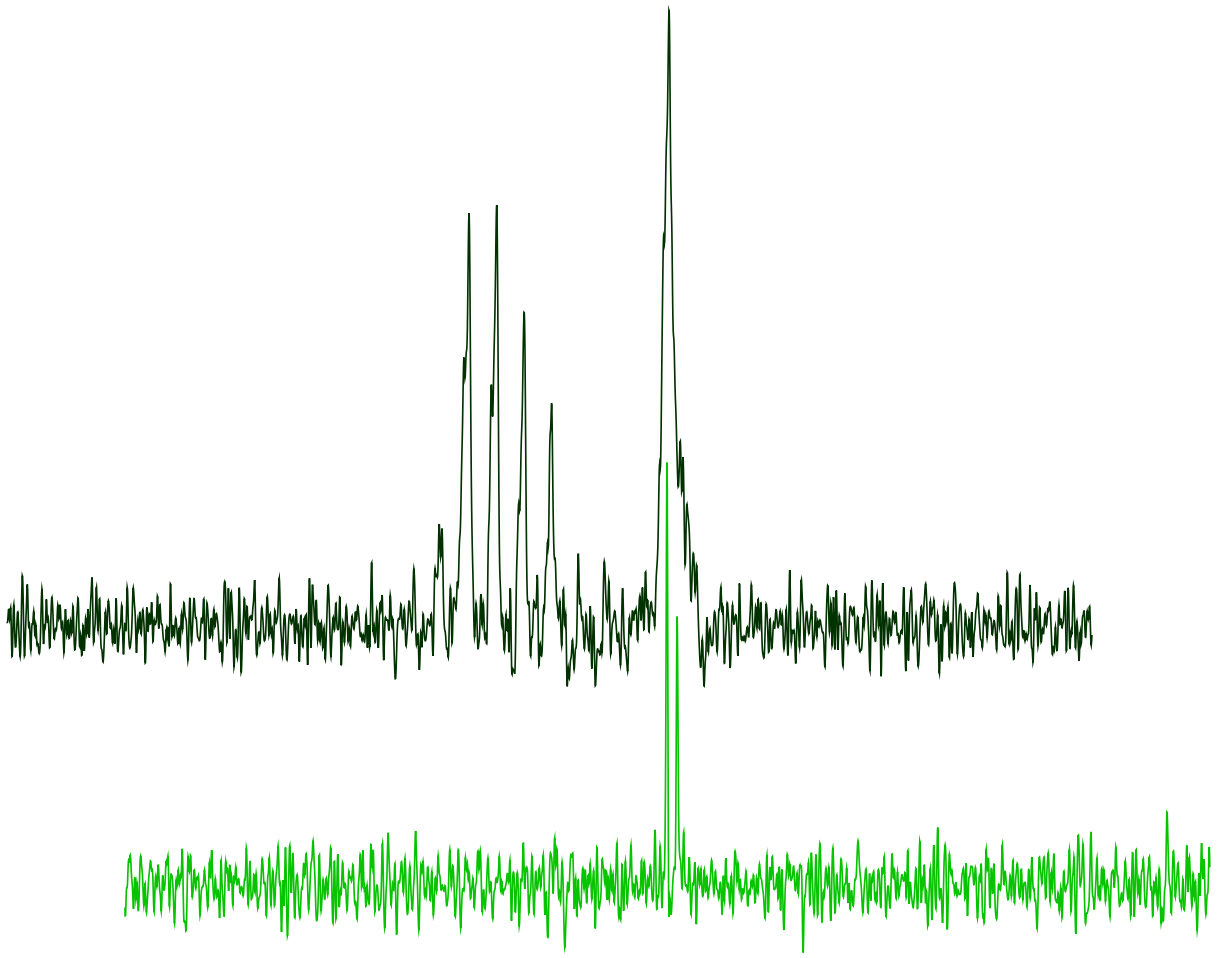

Figure 4.8: Comparison of a one-pulse and a cross-polarization and decoupling sequence with ^{13}C detected on an alanine sample spinning at 5.5 kHz.

This is what will allow the probe to be used for the more complex experiments required for studies of structure and dynamics in oriented samples.

Chapter 5

Conclusion

The design of this probe has been optimized for the study of oriented biomacromolecules. The coaxial arrangement of the modified Alderman-Grant coil and the variable-pitch solenoid allows long decoupling pulses on the ^{1}H channel and efficient detection on the ^{13}C/^{2}H/^{15}N channels. The homogeneity of the coils and the tuning of the channels have been refined to allow the multi-day experiments required for structural characterization. The inclusion of a full-power ^{2}H channel with the traditional ^{1}H/^{13}C/^{15}N will allow a range of alignment studies as well as higher-dimensional experiments that fully utilize the expensive deuteration of biomacromolecules commonly used in solid-state NMR.

Bibliography

[1] Tatyana I. Igumenova, Ann E. McDermott, Kurt W. Zilm, Rachel W. Martin, Eric K. Paulson, and A. Joshua Wand. Assignments of carbon nmr resonances for microcrystalline ubiquitin. *Journal of the American Chemical Society*, 126(21):6720–6727, 2004. PMID: 15161300.

[2] Malcolm H. Levitt. *Spin Dynamics*. John Wiley & Sons, Ltd, Chichester, 2001.

[3] Jane S. Richardson. The anatomy and taxonomy of protein structure. Advances in Protein Chemistry, pages 167 – 339. Academic Press, 1981.

[4] Michel E. Goldberg. The second translation of the genetic message: protein folding and assembly. *Trends in Biochemical Sciences*, 10(10):388 – 391, 1985.

[5] C. M. Dobson. Protein folding and its links with human disease. In *From Protein Folding to New Enzymes*, Biochemical Society Symposium, pages 1–26. 2001. 68 BS87R.

[6] Philip J. Thomas, Bao-He Qu, and Peter L. Pedersen. Defective protein folding as a basis of human disease. *Trends in Biochemical Sciences*, 20(11):456 – 459, 1995.

[7] S.Y. TAN and M.B. PEPYS. Amyloidosis. *Histopathology*, 25(5):403–414, 1994.

[8] Peter Csermely. Chaperone overload is a possible contributor to 'civilization diseases'. *Trends in Genetics*, 17(12):701 – 704, 2001.

[9] J. P. Rosenbusch. Stability of membrane proteins: Relevance for the selection of appropriate methods for high-resolution structure determinations. *Journal of Structural Biology*, 136(2):144–157, 2001.

[10] R. S. Prosser, F. Evanics, J. L. Kitevski, and M. S. Al-Abdul-Wahid. Current applications of bicelles in nmr studies of membrane-associated amphiphiles and proteins. *Biochemistry*, 45(28):8453–8465, Jul 2006.

[11] Francesca M. Marassi. Nmr of peptides and proteins in oriented membranes. *Concepts in Magnetic Resonance*, 14:212–224, 2002.

[12] N. C. Nielsen, A. Malmendal, and T. Vosegaard. Techniques and applications of nmr to membrane proteins (review). *Molecular Membrane Biology*, 21(3):129–141, 2004.

[13] S. J. Opella and F. M. Marassi. Structure determination of membrane proteins by nmr spectroscopy. *Chemical Reviews*, 104(8):3587–3606, 2004.

[14] Felix Bloch. Nuclear induction. *Physical Review*, 70:460–474, 1946.

[15] H. C. Torrey. Bloch equations with diffusion terms. *Physical Review*, 104:563–565, 1956.

[16] U. Haeberlen. Anisotropy of Chemical-Shift of Protons in Hydrogen-Bonds. *Berichte Der Bunsen-Gesellschaft-Physical Chemistry Chemical Physics*, 79(11):1013–1015, 1975. Times Cited: 6.

[17] M. Mehring and J. S. Waugh. Magic-angle nmr experiments in solids. *Phys. Rev. B*, 5(9):3459–3471, May 1972.

[18] E. R. Andrew, A. Bradbury, and R. G. Eades. Nuclear magnetic resonance spectra from a crystal rotated at high speed. *Nature*, 182(4650):1659–1659, 1958.

[19] G.A. Morris and R. Freeman. Enhancement of nuclear magnetic resonance signals by polarization transfer. *Journal of the Americal Chemical Society*, 101:760–762, 1979.

[20] A. Pines, J. S. Waugh, and M. G. Gibby. Proton-enhanced nuclear induction spectroscopy - method for high-resolution NMR of dilute spins in solids. *Journal of Chemical Physics*, 56(4):1776, 1972.

[21] P. Caravatti, G. Bodenhausen, and R. R. Ernst. Heteronuclear solid-state correlation spectroscopy. *Chemical Physics Letters*, 89:363–367, 1982.

[22] P. Caravatti, L. Braunschweiler, and R. R. Ernst. Heteronuclear correlation spectroscopy in rotating solids. *Chemical Physics Letters*, 100:305–310, 1983.

[23] A. T. Petkova, M. Baldus, M. Belenky, M. Hong, R. G. Griffin, and J. Herzfeld. Backbone and side chain assignment strategies for multiply labeled membrane peptides and proteins in the solid state. *Journal of Magnetic Resonance*, 160(1):1–12, 2003.

[24] K H Gardner and L E Kay. The use of 2H, 13C, 15N multidimensional NMR to study the structure and dynamics of proteins. *Annu Rev Biophys Biomol Struct*, 27:357–406, 1998.

[25] A. E. McDermott, F. J. Creuzet, A. C. Kolbert, and R. G. Griffin. High-Resolution Magic-Angle-Spinning NMR-Spectra of Protons in Deuterated Solids. *Journal of Magnetic Resonance*, 98(2):408–413, 1992.

[26] M. Hologne, V. Chevelkov, and B. Reif. Deuterated peptides and proteins in MAS solid-state NMR. *Progress in Nuclear Magnetic Resonance Spectroscopy*, 48:211–232, 2006.

[27] M. Hologne, K. Faelber, A. Diehl, and B. Reif. Characterization of dynamics of perdeuterated proteins by MAS solid-state NMR. *JACS Communications*, 127(32):11208–11209, March 2005.

[28] Vipin Agarwal, Anne Diehl, Nikolai Skrynnikov, and Bernd Reif*. High resolution 1H detected 1H, 13C correlation spectra in MAS solid-state NMR using deuterated proteins with selective 1H, 2H isotopic labeling of methyl groups. *Journal of the American Chemical Society*, 128(39):12620–12621, 2006.

[29] Tim Doherty and Mei Hong. High-resolution solid-state NMR of anisotropically mobile molecules under very low-power 1H decoupling and moderate magic-angle spinning. *J Magn Reson*, 199(2):225–32, Aug 2009.

[30] Amanda J. Brindley and Rachel W. Martin. Effect of divalent cations on dmpc/dhpc bicelle formation and alignment. *Langmuir*, 28(20):7788–7796, 2012.

[31] S. E. Ashbrook and M. J. Duer. Structural information from quadrupolar nuclei in solid state NMR. *Concepts in Magnetic Resonance Part A*, 28A(3):183–248, 2006.

[32] Christian Fernandez and Marek Pruski. Probing quadrupolar nuclei by solid-state NMR spectroscopy: Recent advances. *Topics in Current Chemistry*, 306:119–188, 2012.

[33] Rebecca A. Shapiro. *Solid- and Solution-State NMR Techniques for the Investigation of Local Ordering in Membrane-Derived Solids via Measurement of Scaled Dipolar Couplings*. Doctor of Philosophy, University of California, Irvine, 2013.

[34] D. S. McNair. Heat-transfer in nmr of conductive samples with radiofrequency decoupling. *Journal of Magnetic Resonance*, 45(3):490–502, 1981. MW683 J MAGN RESON.

[35] J. B. D. de Lacaillerie, B. Jarry, O. Pascui, and D. Reichert. "cooking the sample": Radiofrequency induced heating during solid-state nmr experiments. *Solid State Nuclear Magnetic Resonance*, 28(2-4):225–232, 2005.

[36] John A. Stringer, C.E. Bronniman, C.G. Mullen, D.H. Zhou, S.A. Stellfox, Y. Li, E.H. Williams, and C.M. Rienstra. Reduction of rf-induced sample heating with a scroll coil resonator structure for solid-state nmr probes. *Journal of Magnetic Resonance*, 173:40–48, 2005.

[37] Rachel W. Martin, John E. Kelly, and Kelsey A. Collier. Spatial reorientation experiments for nmr of solids and partially oriented liquids. *Progress in Nuclear Magnetic Resonance Spectroscopy*, 90–91:92–122, 2015.

[38] Christopher V. Grant, Chin H. Wu, and Stanley J. Opella. Probes for high field solid-state nmr of lossy biological samples. *Journal of Magnetic Resonance*, 204(2):180–188, 2010.

[39] Seth A. McNeill, Peter L. Gor'kov, Kiran Shetty, William W. Brey, and Joanna R. Long. A low-e magic angle spinning probe for biological solid state nmr at 750xa0;mhz. *Journal of Magnetic Resonance*, 197(2):135–144, 2009.

[40] F. David Doty, Jatin Kulkarni, Christopher Turner, George Entzminger, and Anthony Bielecki. Using a cross-coil to reduce rf heating by an order of magnitude in triple-resonance multinuclear mas at high fields. *Journal of Magnetic Resonance*, 182(2):239–253, 2006.

[41] Donald W. Alderman and David M. Grant. An efficient decoupler coil design which reduces heating in conductive samples in superconducting spectrometers. *Journal of Magnetic Resonance (1969)*, 36(3):447–451, 1979.

[42] S. Idziak and U. Haeberlen. Design and construction of a high homogeneity rf coil for solid-state multiple-pulse nmr. *Journal of Magnetic Resonance*, 50(2):281–288, 1982. Times Cited: 41.

[43] D.I. Hoult and R.E. Richards. The signal-to-noise ratio of the nuclear magnetic resonance experiment. *Journal of Magnetic Resonance*, 24:71–85, 1976.

[44] Christopher V. Grant, Yuan Yang, Mira Glibowicka, Chin H. Wu, Sang Ho Park, Charles M. Deber, and Stanley J. Opella. A modified alderman–grant coil makes possible an efficient cross-coil probe for high field solid-state nmr of lossy biological samples. *Journal of Magnetic Resonance*, 201(1):87–92, 2009.

[45] Eric K Paulson, Rachel W Martin, and Kurt W Zilm. Cross polarization, radio frequency field homogeneity, and circuit balancing in high field solid state nmr probes. *Journal of Magnetic Resonance*, 171(2):314–23, Dec 2004.

[46] V. R. Cross, R. K. Hester, and J. S. Waugh. Single Coil Probe With Transmission-Line Tuning For Nuclear Magnetic Double-Resonance. *Review of Scientific Instruments*, 47(12):1486–1488, 1976.

[47] F. M. Schabauer and R. Blumkin. Thermal resistance, power dissipation, and current rating for ceramic and porcelain multilayer capacitors. *RF Design Magazine*, (May/June and July/August), 1981.

[48] G. Kent and M. Ingalls. High frequency performance of multilayer capacitors - comments. *IEEE Transactions On Microwave Theory and Techniques*, 45(2):311–312, 1997. English Letter FEB IEEE TRANS MICROWAVE THEORY.

[49] Willis Jackson. *High Frequency Transmission Lines*. Methuen Monographs on Physical Subjects. Methuen and Co. LTD, London, 1944.

[50] John A. Stringer and Gary P. Drobny. Methods for the analysis and design of a solid state nuclear magnetic resonance probe. *Review of Scientific Instruments*, 69(9):3384–3391, 1998.

[51] Rachel W. Martin, Eric K. Paulson, and Kurt W. Zilm. Design of a triple resonance magic angle sample spinning probe for high field solid state nuclear magnetic resonance. *Review of Scientific Instruments*, 74(6):3045–3061, 2003.

[52] S. Kan, M. Fan, and J. Courtieu. A single-coil triple resonance probe for nmr experiments. *Review of Scientific Instruments*, 51(7):887–890, 1980.

[53] Joël Mispelter, Mihaela Lupu, and André Briguet. *NMR Probeheads for Biophysical and Biomedical Experiments*. Imperial College Press, London, 2006.